nature communications

Article

https://doi.org/10.1038/s41467-024-50806-y

Tregs delivered post-myocardial infarction adopt an injury-specific phenotype promoting cardiac repair via macrophages in mice

Received: 30 October 2023

Accepted: 22 July 2024

Published online: 01 August 2024

Check for updates

Yasmin K. Alshoubaki[1], Bhavana Nayer[1], Yen-Zhen Lu[1], Ekaterina Salimova[2], Sin Nee Lau[1], Jean L. Tan[1], Daniela Amann-Zalcenstein[3,4], Peter F. Hickey[3,4], Gonzalo del Monte-Nieto[1,5], Ajithkumar Vasanthakumar[6,7,8] & Mikaël M. Martino[1,5]

Regulatory T cells (Tregs) are key immune regulators that have shown promise in enhancing cardiac repair post-MI, although the mechanisms remain elusive. Here, we show that rapidly increasing Treg number in the circulation post-MI via systemic administration of exogenous Tregs improves cardiac function in male mice, by limiting cardiomyocyte death and reducing fibrosis. Mechanistically, exogenous Tregs quickly home to the infarcted heart and adopt an injury-specific transcriptome that mediates repair by modulating monocytes/macrophages. Specially, Tregs lead to a reduction in pro-inflammatory Ly6C^{Hi} CCR2^{+} monocytes/macrophages accompanied by a rapid shift of macrophages towards a pro-repair phenotype. Additionally, exogenous Treg-derived factors, including nidogen-1 and IL-10, along with a decrease in cardiac CD8^{+} T cell number, mediate the reduction of the pro-inflammatory monocyte/macrophage subset in the heart. Supporting the pivotal role of IL-10, exogenous Tregs knocked out for IL-10 lose their pro-repair capabilities. Together, this study highlights the beneficial use of a Treg-based therapeutic approach for cardiac repair with important mechanistic insights that could facilitate the development of novel immunotherapies for MI.

Myocardial infarction (MI) is the most common form of acute cardiac injury and is a leading cause of global mortality. MI generally results from a blockage in the coronary arteries which reduces blood flow to the downstream ventricular tissue, causing a rapid death of cardiomyocytes. Consequently, the heart undergoes remodelling and the ischemic area forms a scar tissue that impairs the overall contractility of the heart[1]. Angioplasty, stenting, or coronary artery bypass surgery are procedures performed as soon as possible following MI, in order to restore blood flow to the ischemic tissue. Several other treatments have been investigated to reduce inflammation, promote

[1]European Molecular Biology Laboratory Australia, Australian Regenerative Medicine Institute, Monash University, Melbourne, Australia. [2]Monash Biomedical Imaging, Monash University, Melbourne, Australia. [3]Advanced Genomics Facility, Advanced Technology and Biology Division, The Walter and Eliza Hall Institute of Medical Research, Parkville, Australia. [4]Department of Medical Biology, University of Melbourne, Melbourne, Australia. [5]Victorian Heart Institute, Monash University, Victorian Heart Hospital, Melbourne, Australia. [6]Olivia Newton-John Cancer Research Institute, Heidelberg, Australia. [7]La Trobe University, Bundoora, Australia. [8]Department of Microbiology and Immunology, University of Melbourne, Melbourne, Australia. e-mail: mikael.martino@monash.edu

angiogenesis, and decrease fibrosis, including stem cell-based therapies and the administration of protein therapeutics[2–4]. However, many of those approaches have shown relatively modest effectiveness.

It is now well recognised that the immune system plays a pivotal role in cardiac repair. Therefore, therapeutic strategies that modulate the immune components involved in the response to MI are being explored. These strategies often rely on the use of stem cells or protein therapeutics that target the inflammatory pathways exacerbated post-MI[5,6]. In particular, approaches that target innate immune cells such as monocytes and macrophages (Mo/MΦ) have been investigated, as these cells are critical in cardiac remodelling[7]. Indeed, Mo/MΦ are among the first immune cells to accumulate at the site of injury and they play an important role in the removal of dead cells and debris[7]. In addition, once activated in the MI area, Mo/MΦ take on different polarisation states that positively or negatively regulate the cardiac repair process[7,8]. Thus, controlling Mo/MΦ phenotypes post-MI could be an effective approach to promote cardiac repair and limit fibrosis. More recently, it has been recognised that adaptive immune cells, such as T cells, are important regulators of cardiac repair outcomes following MI. For example, it has been shown that cytotoxic $CD8^+$ T cells in the infarcted tissue produce pro-inflammatory cytokines, which further promote inflammation and tissue damage[9]. Additionally, $CD8^+$ T cells have been shown to have a cytotoxic effect on cells that are undergoing necrosis or apoptosis[9].

Regulatory T cells are another type of T cells that have been shown to positively impact cardiac repair[4,10–14]. For instance, studies have shown that Tregs modulate the cardiac immune response following MI, by reducing $CD8^+$ T cells[14] and modulating Mo/MΦ[13]. In addition, they may exercise a direct protective or pro-regenerative effect on cardiac cells such as fibroblasts, endothelial cells, and cardiomyocytes[4,15,16]. Therefore, utilising Tregs or pharmacologically controlling endogenous Tregs could be an attractive therapeutic approach following MI[16–18]. Nevertheless, while the positive impact of Tregs on cardiac function is relatively clear, the specific mechanisms by which Tregs modulate immune cells and the overall inflammatory microenvironment at the MI site, as well as the timeframe in which they are critical, remain unclear. In this study, we used mouse models to investigate whether rapidly increasing circulating Treg numbers post-MI via exogenous Treg administration is an effective therapeutic strategy to enhance cardiac repair outcomes. Furthermore, we uncovered key mechanisms by which exogenous Tregs modulate immune cell populations to promote cardiac repair.

Results

Systemic delivery of exogenous Tregs promotes cardiac repair following MI

To induce MI in the mouse we performed a permanent left coronary artery (LCA) ligation. We first confirmed the importance of Tregs during cardiac repair by using the *Foxp3*$^{DTR/GFP}$ mouse in which diphtheria toxin administration depletes $Foxp3^+$ expressing cells (Supplementary Fig. 1a–c). As previously shown, Treg ablation resulted in a significantly reduced ejection fraction and increased fibrosis in the heart four weeks post-MI, indicating a worsened function and contractility of the left ventricle (Supplementary Fig. 1d–g). Since Treg depletion results in a deteriorated cardiac outcome post-MI, we hypothesised that rapidly increasing the number of Tregs in the circulation after MI would improve cardiac repair. To increase the number of Tregs in the circulation following MI, we systemically injected one million Tregs purified from *Foxp3*$^{DTR/GFP}$ mouse spleens, one day post-MI, and assessed the cardiac repair outcome at baseline, one and four weeks after MI (Fig. 1a and Supplementary Fig. 2a). We observed that treatment with exogenous Tregs results in a significant improvement of cardiac repair, as evidenced by ameliorated ejection fraction, reduced end diastolic volume, and reduced fibrosis of the left ventricle (Fig. 1b–f), increased end-systolic posterior and anterior wall thickness and reduced internal diameter of the left ventricle in systole (Supplementary Fig. 3a).

Since MI induces the death of cardiomyocytes, we examined if the delivery of exogenous Tregs promoted cardiomyocyte survival by performing a TUNEL assay three days post-treatment. Remarkably,

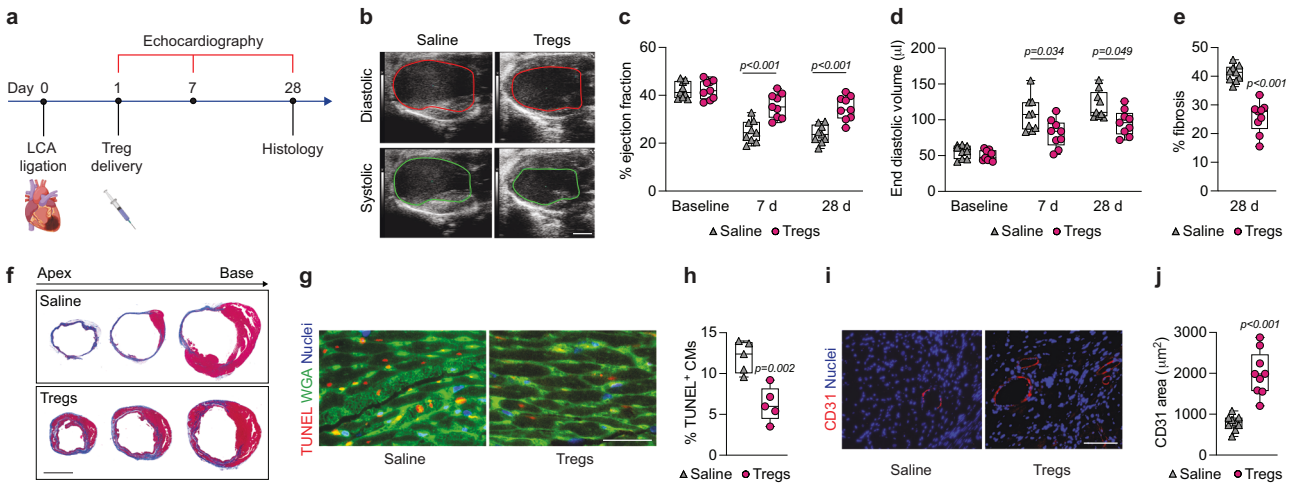

Fig. 1 | Systemic delivery of exogenous Tregs post-MI improves the cardiac repair outcome. a–j LCA ligation was performed in wild-type (wt) mice. Mice received a systemic injection of saline or Tregs, 1 day after MI. The experimental design is shown in (**a**). **b** Representative parasternal long-axis views of the left ventricles. Scale bar: 2 mm. **c** Left ventricular ejection fraction ($n = 9$). **d** Left ventricular end diastolic volume in µl measured by echocardiography at baseline, 7 and 28 days post-MI ($n = 9$). **e** Quantification of fibrosis by histology expressed as percentage of the left ventricular area ($n = 9$). **f** Representative histology of whole transverse heart sections from apex to base, after Masson's Trichrome staining, 28 days post-MI. Scale bar: 2 mm. **g** Representative sections of the heart 3 days post-treatment with staining of apoptotic cells in red (TUNEL assay), cell border (wheat germ agglutinin, WGA; in green), and nuclei in blue (in blue). Scale bar: 100 µm. **h** Quantification of $TUNEL^+$ cardiomyocytes (CMs) ($n = 5$). **i** Representative immunostaining of heart sections for endothelial cells (CD31, in red)) and nuclei (in blue) 28 days post-MI. Scale bar: 100 µm. **j** Quantification of immunostaining for CD31 ($n = 9$). For all graphs, boxes show median (centre line) and interquartile range (edges), whiskers show the range of values and dots represent individual data points. Two-way ANOVA with Bonferroni *post-hoc* test for pair-wise comparisons was used to compare the groups in (**c**, **d**). Two-tailed Student's *t*-test was used to compare the groups in (**e**, **h**, **j**). *P*-values are indicated. Panel (**a**) created with BioRender.com released under a Creative Commons Attribution-NonCommercial-NoDerivs 4.0 International license (https://creativecommons.org/licenses/by-nc-nd/4.0/deed.en).

https://doi.org/10.1038/s41467-024-50806-y

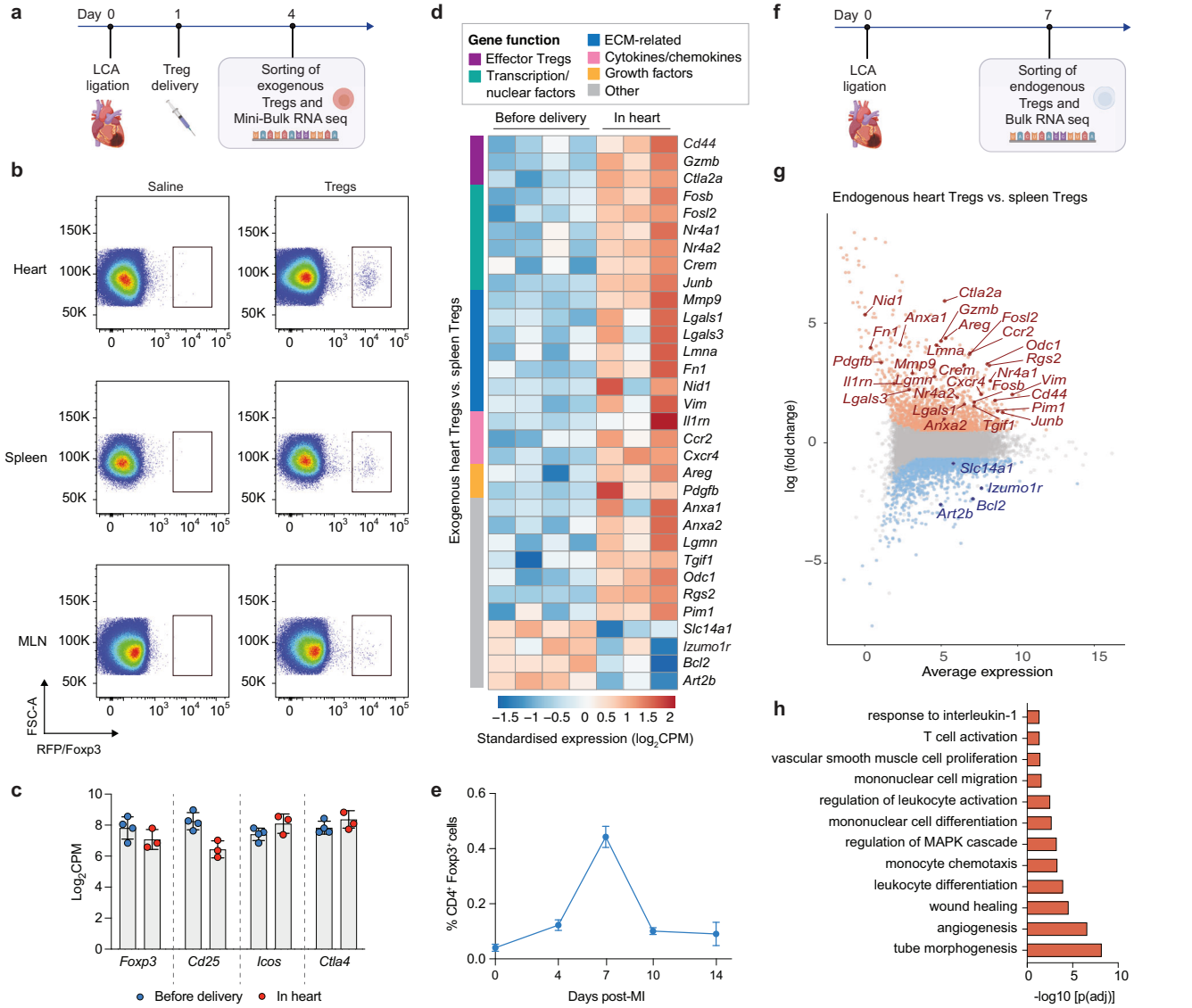

Fig. 2 | Exogenous Tregs homing to the heart adopt an injury-specific transcription profile similar to endogenous heart Tregs. a–d Mice received a systemic injection of saline or Tregs (from *Foxp3*$^{IRES\text{-}mRFP}$ mice), 1 day post-MI. Four days post-MI, the delivered red-fluorescent protein (RFP) positive Tregs were sorted from the heart, spleen, and mediastinum lymph nodes (MLN) for bulk RNA sequencing. The experimental timeline is shown in (**a**). **b** Flow cytometry plots showing RFP$^+$ Tregs gated from total CD3$^+$ cells in the heart, spleen and MLN 4 days post-MI. **c** Count per million (CPM) plots depicting gene expression levels of classic Treg markers in exogenous Tregs before delivery and exogenous Tregs recovered from the heart (data are presented as mean ± SD, $n = 3$–4/group). **d** Heat map of selected significantly upregulated genes depicting standardised gene expression values in exogenous Tregs before delivery and exogenous Tregs recovered from the heart. Genes are classified according to main known function indicated by the coloured tab next to the heat map. **e** Accumulation kinetic of endogenous Tregs in the myocardium post-MI. Data are presented as mean ± SD ($n = 4$). **f–h** Endogenous heart Tregs were sorted and sequenced 7 days post-MI, along with Tregs from spleens of uninjured mice. The experimental timeline is shown in (**f**). **g** MA-plot of differentially expressed genes (FDR < 0.05, fold change > |1.5 |) in Tregs sorted from the infarcted heart vs. Tregs from uninjured spleen. Common genes between the endogenous heart Tregs and the exogenous Tregs in (**d**) are labelled. Biological replicates are shown and each replicate comes from a pool of > 2 injuries. **h** GO analysis showing enriched terms from all commonly upregulated genes between endogenous and exogenous Tregs sorted from the heart (FDR < 0.01, adjusted by Benjamini-Hochberg correction). Panels (**a**, **f**) created with BioRender.com released under a Creative Commons Attribution-NonCommercial-NoDerivs 4.0 International license (https://creativecommons.org/licenses/by-nc-nd/4.0/deed.en).

exogenous Tregs reduced cardiomyocyte cell death in the infarct zone and border zone of the left ventricle (Fig. 1g, h). Then, given that vascularisation within the MI area is critical for proper repair, we assessed the extent of vascularisation by immunostaining for the endothelial cell marker CD31 four weeks post-treatment. Interestingly, we found that mice receiving Tregs had increased blood vessel density in the infarct zone (Fig. 1i, j). Lastly, we evaluated whether Treg delivery could promote cardiomyocyte proliferation by performing immunostaining of the mitosis marker phospho-histone 3 (pH3) seven days post-MI. Exogenous Tregs did not significantly improve cardiomyocyte proliferation in comparison to saline control (Supplementary Fig. 3b, c).

Exogenous Tregs home to the ischemic myocardium and express an injury-specific transcriptome

To determine the pharmacokinetics of exogenous Tregs following delivery, we used Tregs from *Foxp3*$^{IRES\text{-}mRFP}$ mice spleens as they express the very bright fluorescent protein RFP (Fig. 2a, Supplementary Fig. 2b). We found that exogenous Tregs accumulate in the heart within the first day following delivery, and RFP$^+$ cells were also

detected to some extent in the spleen and mediastinal lymph nodes (MLN) up to seven days post-treatment (Fig. 2b, Supplementary Fig. 4). To gain insights on the mechanisms by which exogenous Tregs promote cardiac repair, we recovered RFP$^+$ Tregs from the heart and lymphoid organs three days post-treatment (four days post-MI) by cell sorting (Supplementary Fig. 2d). We then performed mini-bulk RNA sequencing on RFP$^+$ Tregs before delivery and on RFP$^+$ Tregs recovered from the heart, MLN and spleen. The exogenous RFP$^+$ Tregs recovered from all tissues expressed classic Treg markers such as *Foxp3, Icos, Ctla4* and *Cd25* to a similar level compared to Tregs before delivery, confirming that the delivered Tregs maintained their Treg identity after systemic administration (Fig. 2c, Supplementary Fig. 7a). Remarkably, we found that the Tregs recovered from the heart had a stark gene expression profile change in comparison to their state before delivery, as well as compared to Tregs recovered from the spleen and MLN. This indicated that the exogenous Tregs that home to the heart following MI acquire a unique injury-specific transcriptome (Supplementary Fig. 5). Changes in recovered heart Tregs are represented by an MA-plot depicting global differential gene expression and a heat map showing selected differentially expressed genes (DEGs) compared to Tregs before delivery (FDR < 0.05, fold change > |1.5|) (Fig. 2d and Supplementary Fig. 6). These specific genes were highlighted due to their previously known role in mediating Treg response to inflammation and injury[19]. For example, among the DEGs were effector Treg genes like *Gzmb*, *Cd44*, and *Ctla2a*; extracellular matrix (ECM)-related genes including *Mmp9*, *Lgals1*, *Lgals3*, *Fn1*, and *Nid1*; cytokines and chemokine genes like *Il1rn* and *Cxcr4*; growth factors such as *Areg* and *Pdgfb*; as well as *Anxa1* and *Anxa2*. Exogenous Tregs recovered from the heart also differentially expressed other genes in comparison to their pre-delivery state (Supplementary Data 1). In contrast to exogenous Tregs recovered from the heart, Tregs recovered from the MLN and spleen had a slightly different gene expression profile compared to their state before delivery (Supplementary Fig. 5, Supplementary Data 2 and Supplementary Data 3). These DEGs included the upregulation of some transcription factors known to regulate Treg lineage maintenance and support Treg effector functions, such as *Junb*[20], *Nr4a1*[21] and *Nr4a2*[22] (Supplementary Fig. 7b).

To further understand the molecular changes occurring in the exogenous Tregs homing to the heart, we compared them with endogenous Tregs that naturally accumulate in the heart post-MI. First, we monitored the kinetics of endogenous Treg accumulation in the infarct zone and observed that Tregs peaked one week post-MI (Fig. 2e). Thus, using the *Foxp3*$^{DTR/GFP}$ mice, we sorted endogenous GFP$^+$ Tregs from the heart seven days post-MI as well as Tregs from the spleen of uninjured mice and performed bulk RNA sequencing (Fig. 2f, Supplementary Fig. 2e). Endogenous heart Tregs displayed a stark gene expression profile change in comparison to spleen Tregs and showed a significant upregulation of most genes that we had observed with the exogenous RFP$^+$ Tregs recovered from the heart, as represented on the MA-plot (Fig. 2g and Supplementary Fig. 8). Moreover, endogenous heart Tregs expressed additional DEGs (FDR < 0.05), some of which were also highly expressed (with a fold change >2) in exogenous Tregs, albeit not significantly (Supplementary Fig. 9a, b and Supplementary Data 4). To gain insights into the possible mechanisms by which Tregs support cardiac repair, we performed gene ontology (GO) analysis on all overlapping upregulated genes between endogenous heart Tregs and exogenous Tregs recovered from the heart as they are likely to be the most relevant in characterising the biological processes that Tregs modulate (Supplementary Data 5). The analysis revealed biological processes related to tissue repair and immune modulation such as angiogenesis and tube morphogenesis, wound healing, and T cell activation (Fig. 2h). Taken together, these data show that exogenous Tregs homed to the heart post-MI, and quickly adopted a unique injury-specific transcriptome that was akin to that of pro-repair endogenous heart Tregs.

The pro-repair effect of exogenous Tregs depends on Mo/MΦ

As one of the main functions of Tregs is to modulate other immune cells, we explored the effect of exogenous Tregs on immune cell subsets in the infarcted area post-MI. Flow cytometry was used to analyse changes in Mo/MΦ (CD11b$^+$/F4/80$^+$ cells), pro-repair Mo/MΦ (CD11b$^+$/F4/80$^+$/CD206^{Hi} cells), neutrophils (Ly6G$^+$ cells) and T cells (CD3$^+$/CD8$^+$, CD3$^+$/CD4$^+$) on days 4, 7 and 10 post-MI (Fig. 3a, Supplementary Fig. 10a, c). Compared to the saline group, the number of neutrophils and CD4$^+$ T cells remained unchanged in response to exogenous Treg treatment (Supplementary Fig. 10d). In addition, while the total Mo/MΦ number was significantly reduced on day 4 post-MI in the Treg-treated animals, the reduction was not observed on days 7 and 10. Most interestingly however, the expression of the pro-repair marker CD206 on the total Mo/MΦ population was significantly higher in Treg-treated animals on days 7 and 10 (Fig. 3b). In line with this observation, the number of Mo/MΦ expressing high levels of CD206$^+$ was also significantly higher (Supplementary Fig. 10d), suggesting that Mo/MΦ in Treg-treated animals polarised towards a pro-repair phenotype more rapidly. In addition, the number of cytotoxic CD8$^+$ T cells was significantly reduced in the Treg-treated group on days 4, 7 and 10 post-MI (Fig. 3b). Overall, these immune profile changes in the infarcted area suggested that exogenous Tregs induce an anti-inflammatory environment at an early-stage post-MI.

Having observed the modulation of Mo/MΦ in the heart by exogenous Tregs, we investigated the extent to which the pro-repair effect of Tregs depended on Mo/MΦ. For this purpose, we used clodronate liposomes, a well-known method to deplete Mo/MΦ[23–25], which we administered to the mice over a seven-day period (Fig. 3c). On day 4 post-MI the Mo/MΦ were confirmed to be ablated in the infarct zone, blood, and spleen (Supplementary Fig. 11). As previously reported[23–25], Mo/MΦ depletion with clodronate liposomes did not significantly impact cardiac function compared to the saline-only group. Furthermore, the administration of exogenous Tregs did not enhance cardiac repair on days 7 and 28 post-MI in the absence of Mo/MΦ, compared to the saline control group also treated with clodronate liposomes (Fig. 3d–g). Thus, these results strongly suggested that exogenous Tregs exert their pro-repair effect via Mo/MΦ.

Mo/MΦ acquire a pro-repair gene expression profile in response to exogenous Tregs

To gain insights on the molecular mechanisms by which exogenous Tregs modulate Mo/MΦ in the heart, we isolated Mo/MΦ from the infarct zone on days 4 and 7 post-MI from both saline and Treg-treated groups and performed mini-bulk RNA sequencing[26] (Fig. 4a, Supplementary Fig. 12). In comparison to the saline group, Mo/MΦ sorted four days post-MI showed some DEGs (FDR < 0.05) in response to Treg treatment (Supplementary Data 6), including significantly upregulated ECM-related genes (*Postn* and *Sparc*), along with the growth factor *Igf1;* as well as downregulated the matrix metalloproteinases *Mmp9* and the inflammatory cytokine *Il1a* (Fig. 4b). In contrast, Mo/MΦ from Treg-treated mice sorted seven days post-MI showed a stark difference in their gene expression profile (Supplementary Data 7), and significantly upregulated genes associated with a pro-repair and resident macrophage phenotype. For example, these genes included *Mrc1 (Cd206)*, *Csf1r*, *Lyve1*, *Cd163* and *Apoe*. In addition, Mo/MΦ upregulated ECM-related genes such as *Thbs1, Sparc, Col4a2* as well as other pro-repair genes such as *Tmsb4x* (Fig. 4b). Using all the DEGs, we then performed a combined pathway analysis of Mo/MΦ sorted four and seven days post-MI in response to exogenous Treg treatment. We identified upregulated GO biological processes related to positive regulation of myeloid leukocyte differentiation, IL-10 production, and cardiac muscle tissue growth, whilst downregulated pathways included leukocyte migration and inflammatory response (Fig. 4c). The genes depicting the pathways are represented in a gene-concept network plot (Supplementary Fig. 13). To further validate the Mo/MΦ shift

https://doi.org/10.1038/s41467-024-50806-y

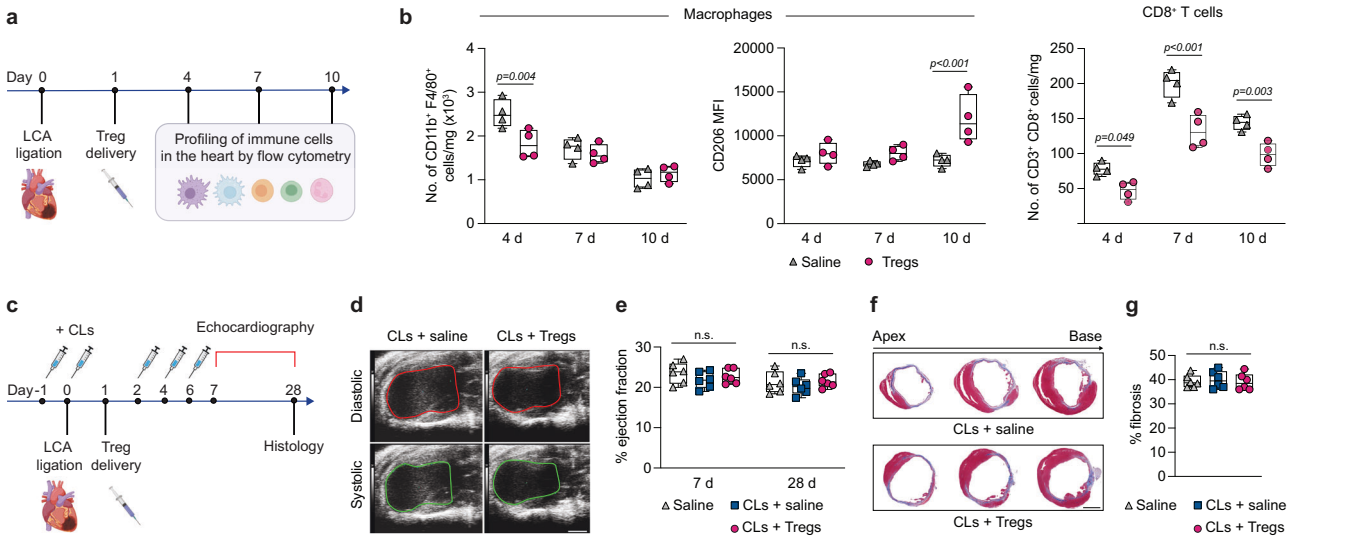

Fig. 3 | The pro-repair effect of exogenous Tregs depends on Mo/MΦ. a, b Wild-type (wt) mice received saline or Tregs 1 day post-MI. Immune cells in the infarct zone were analysed by flow cytometry on days 4, 7 and 10 post-MI. The experimental design is shown in (**a**). **b** Number (No.) of Mo/MΦ ($CD11b^+$, $F4/80^+$ cells) per mg of scar tissue, $CD206^+$ expression in Mo/MΦ (represented by the geometric mean fluorescence intensity, MFI), and number of cytotoxic T cells per mg of scar tissue ($n = 4$). **c**–**g** Mice received saline or were depleted of Mo/MΦ using clodronate liposomes (CLs) prior to receiving saline or Tregs on day 1 post-MI. The experimental design is shown in (**c**). **d** Representative parasternal long-axis views of the left ventricles. The red trace is end-diastolic, and the green is end-systolic. **e** Left ventricular ejection fraction measured by echocardiography 7 and 28 days post-MI ($n = 6$). **f** Representative histology of whole transverse heart sections from apex to base stained with Masson's Trichrome staining, 28 days post-MI. Scale bar: 2 mm. **g** Quantification of fibrosis by histology expressed as percentage of the left ventricle ($n = 6$). For all graphs, boxes show median (centre line) and interquartile range (edges), whiskers show the range of values and dots represent individual data points. Two-way ANOVA with Bonferroni *post-hoc* test for pair-wise comparisons was used to compare the groups in (**b**, **e**). One-way ANOVA with Bonferroni *post-hoc* test for pair-wise comparisons was used to compare the groups in (**g**). *P* values are indicated, n.s. indicates non-significant. Panels (**a**, **c**) created with BioRender.com released under a Creative Commons Attribution-NonCommercial-NoDerivs 4.0 International license (https://creativecommons.org/licenses/by-nc-nd/4.0/deed.en).

towards a pro-repair phenotype, we performed immunostaining on cardiac macrophages ($F4/80^+$ cells) to assess protein expression levels of the surface markers CD206, CD163, LYVE1, and the ECM protein SPARC. Compared to saline treatment, all these proteins showed significantly higher signals in $F4/80^+$ cells from Treg-treated mice seven days post-MI (Fig. 4d, e). Taken together, these results indicated that exogenous Treg administration prompt Mo/MΦ to adopt a pro-repair profile favourable of cardiac repair.

The absence of Tregs after MI leads to a pro-inflammatory phenotype in cardiac Mo/MΦ

To further delineate the mechanisms by which exogenous Tregs modulate Mo/MΦ, we performed RNA sequencing on infarct zone Mo/MΦ sorted four and seven days post-MI from Treg-depleted animals, as this mimicked the opposite situation to the Treg treatment (Fig. 5a). Compared to the non-depleted controls group, Mo/MΦ sorted four and seven days post-MI fromTreg-depleted mice showed significant changes (Supplementary Data 8 and Supplementary Data 9). Interestingly, amongst the significantly upregulated genes (FDR < 0.05) was *Ly6c2* (Fig. 5b), which suggests an increase in the proportion of the inflammatory Ly6C high ($Ly6C^{Hi}$) Mo/MΦ subset[27]. This was accompanied by a significant downregulation of resident cardiac macrophage markers *Lyve1* and *Cd163*[28,29], which was opposite to what was observed in Mo/MΦ following exogenous Treg treatment (Figs. 4b and 5b). The expression profile suggested that Tregs control the accumulation of inflammatory Mo/MΦ and their polarisation into an anti-inflammatory and pro-repair phenotype. This was also supported by the observation that Mo/MΦ in Treg-depleted animals downregulated pro-repair genes that were found to be upregulated upon exogenous Treg administration, such as *Thbs1*, *Nr4a1* and *Rbpj* (Figs. 4b and 5b). In addition, Mo/MΦ from Treg-depleted mice showed downregulation of other pro-repair genes such *as Vegfb, Nrp1, Ptma* and *Areg* (Fig. 5b). Using all the DEGs, we then performed a combined pathway analysis of Mo/MΦ from Treg-depleted animals, sorted four and seven days post-MI. We identified upregulated GO biological processes related to the interferon (IFN)-γ pathway, response to IFN-α, IFN-β, and IL-1, as well as monocyte chemotaxis, whilst downregulated pathways included angiogenesis and endothelial cell chemotaxis (Fig. 5c). The genes depicting the pathways are represented in a gene-concept network plot (Supplementary Fig. 14). In summary, these results demonstrated that the absence of Tregs exacerbates the inflammatory response by increasing the proportion of pro-inflammatory Mo/MΦ in the infarct zone post-MI.

Tregs mitigate their effect via the $Ly6C^+$ $CCR2^+$ Mo/MΦ subset

As the $Ly6C^{Hi}$ Mo/MΦ subset is also characterised by high CCR2 expression[27], we used flow cytometry to examine $Ly6C^{Hi}$ $CCR2^+$ Mo/MΦ in the infarct zone following exogenous Treg treatment (Fig. 6a). Remarkably, we found a significant reduction in the number of $Ly6C^{Hi}$ $CCR2^+$ cells two days after Treg delivery, indicating a lower accumulation of this pro-inflammatory Mo/MΦ subset in the heart (Fig. 6b and Supplementary Fig. 10b). Thus, we investigated whether exogenous Treg treatment promoted cardiac repair through the $Ly6C^{Hi}$ $CCR2^+$ subset. To this end, we systemically depleted $CCR2^+$ cells during the first week post-MI using an anti-CCR2 antibody (clone MC21) which inhibits the migration of $CCR2^+$ Mo/MΦ to the heart[30,31] (Fig. 6c, d). Notably, we used a mouse Fc-silent antibody to avoid non-specific effects from the Fc part of the antibody[32]. Firstly, blocking $CCR2^+$ Mo/MΦ accumulation in the heart ameliorated the left ventricular ejection after MI, suggesting that inhibiting the accumulation of $CCR2^+$ Mo/MΦ is beneficial for cardiac repair (Fig. 6e–h). Secondly, exogenous Treg treatment did not significantly improve cardiac repair compared to the antibody-only control group (Fig. 6e–h), implying that exogenous

https://doi.org/10.1038/s41467-024-50806-y

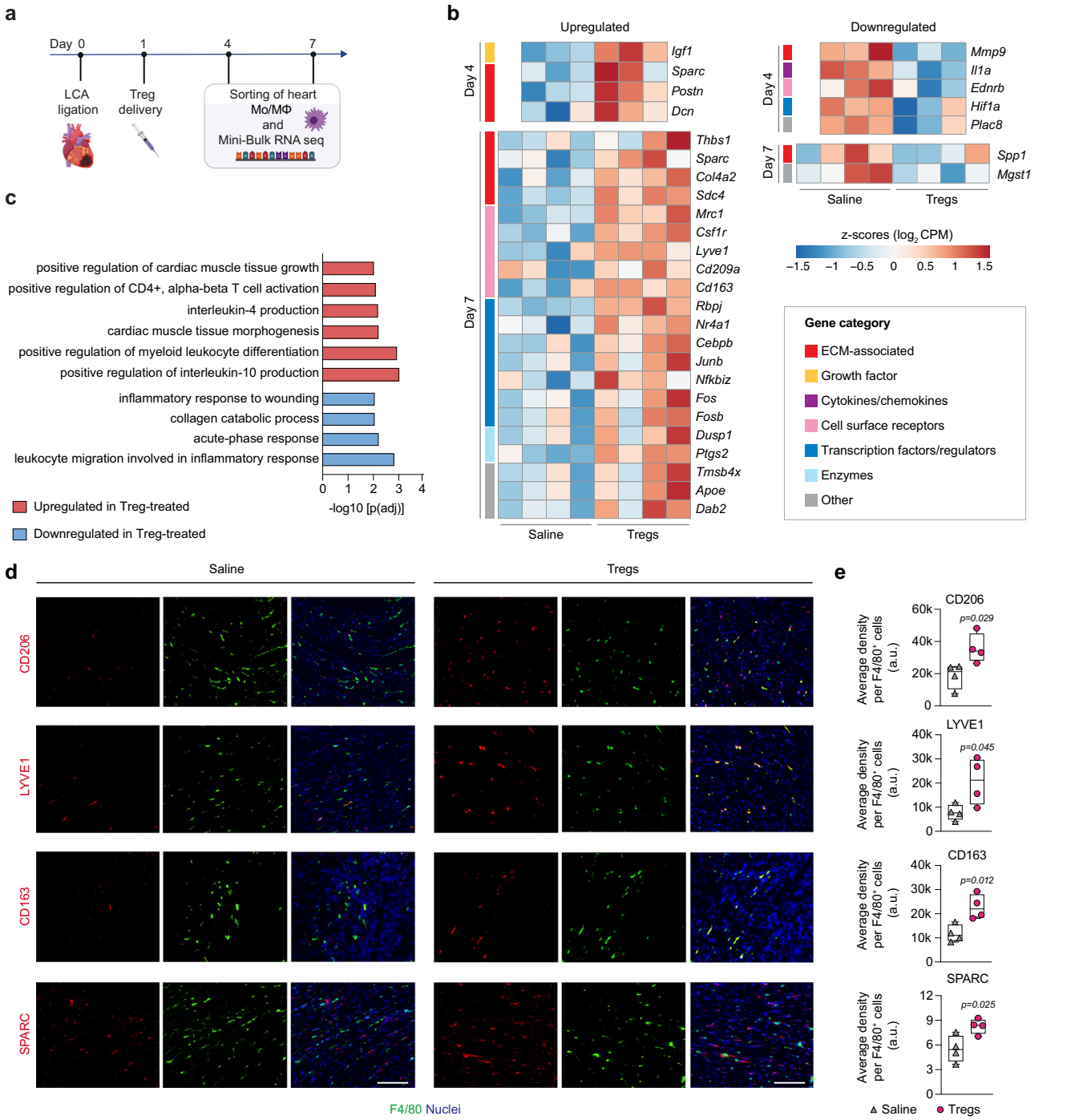

Fig. 4 | Mo/MΦ adopt a pro-repair profile in response to exogenous Tregs. **a**–**c** Endogenous cardiac Mo/MΦ from saline- and Treg-treated groups were sorted and sequenced on days 4 and 7 post-MI ($n = 4$ for saline, $n = 3$ for Tregs). The experimental design is shown in (**a**). **b** Heat map of selected significantly upregulated and downregulated DEGs (FDR < 0.05) depicting standardised gene expression values on days 4 and 7 post-MI (individual biological replicates are shown). Genes are classified according to function with the coloured tab to the left of the heat map. **c** GO enriched terms depicting biological processes in the significantly upregulated and downregulated genes in Mo/MΦ following exogenous Treg treatment from days 4 and 7 post-MI (FDR < 0.01, adjusted by Benjamini-Hochberg correction). **d**, **e** LCA ligation was performed in wild-type mice, followed by a systemic injection of either saline or Tregs 1 day post-MI. Hearts were collected on day 7 post-MI and stained for F4/80 (green) to identify Mo/MΦs, with proteins of interest (CD206, LYVE1, CD163, and SPARC) in red, and nuclei stained in blue. **d** Representative images. Scale bar: 100 µm. **e** Quantification of signal intensity expressed as average raw density per F4/80$^+$ cells ($n = 4$). For all graphs, Boxes show median (centre line) and interquartile range (edges), whiskers show the range of values and dots represent individual data points. Two-tailed Student's *t*-test was used to compare the groups in (**e**). *P* values are indicated. Panel (**a**) created with BioRender.com released under a Creative Commons Attribution-NonCommercial-NoDerivs 4.0 International license (https://creativecommons.org/licenses/by-nc-nd/4.0/deed.en).

Tregs likely exert their reparative effects primarily on the Ly6C^{Hi} CCR2$^+$ subset.

As treatment with Tregs led to a significant reduction in Ly6C^{Hi} CCR2$^+$ Mo/MΦ and CD8$^+$ T cells in the heart, we investigated whether the change in the Ly6C^{Hi} CCR2$^+$ subset was directly mediated by exogenous Treg-derived factors or indirectly as a consequence of reduced CD8$^+$ T cell numbers. To address this, we established an ex vivo culture system using cardiac Mo/MΦ that were sorted three days post-MI

https://doi.org/10.1038/s41467-024-50806-y

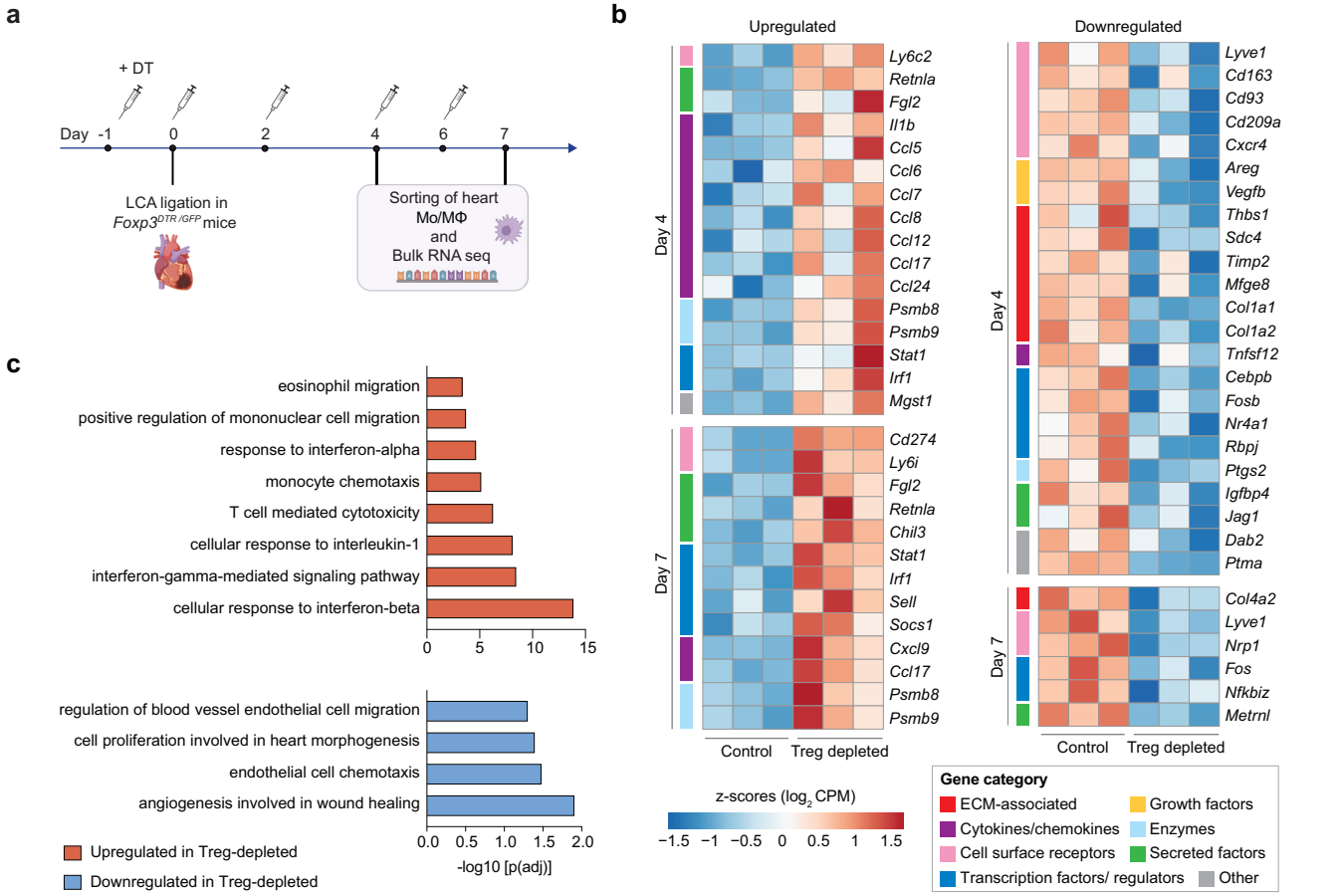

Fig. 5 | The absence of Tregs after MI leads to a pro-inflammatory phenotype in cardiac Mo/MΦ. a–c *Foxp3*$^{DTR/GFP}$ and wild-type control mice received diphtheria toxin (DT) to deplete Tregs in *Foxp3*$^{DTR/GFP}$ mice. MI was induced by LCA ligation and cardiac Mo/MΦ were sorted on days 4 and 7 post-MI for bulk RNA sequencing. The experimental design is shown in (**a**). **b** Heat maps of selected significantly upregulated and downregulated DEGs (FDR < 0.05) depicting standardised gene expression values on days 4 and 7 post-MI (n = 3). Genes are classified according to function with the coloured tab at the bottom of the heat maps. **c** GO analysis depicting enriched biological processes from commonly upregulated and downregulated DEGs in cardiac Mo/MΦs from Treg-depleted mice across both time points (FDR < 0.01, adjusted by Benjamini-Hochberg correction). Panel (**a**) created with BioRender.com released under a Creative Commons Attribution-NonCommercial-NoDerivs 4.0 International license (https://creativecommons.org/licenses/by-nc-nd/4.0/deed.en).

(Fig. 6i). The influence of CD8$^+$ T cell numbers on Ly6C expression was assessed by supplementing the culture with varying amounts of cardiac CD8$^+$ T cells that were co-sorted three days post-MI. We observed a significant decrease in Ly6C expression when the culture had fewer CD8$^+$ T cells, indicating a significant impact of cardiac CD8$^+$ T cells on the pro-inflammatory state of cardiac Mo/MΦ (Fig. 6j). Then, to assess a potential direct effect of exogenous Treg-derived factors, we cultured cardiac Mo/MΦ with IFN-γ to maintain their pro-inflammatory state, and tested the effect of annexin-A1, galectin-1, galectin-3, nidogen-1, and IL-10 on Ly6C expression by flow cytometry (Fig. 6k). These factors were selected as they have been previously shown to influence Mo/MΦ phenotypes[2,33–36] and were expressed by exogenous Tregs in the heart (Fig. 2d and Supplementary Fig. 9b). We observed a significant reduction in Ly6C expression with nidogen-1 and IL-10 treatment (Fig. 6k), indicating that these exogenous Treg-derived factors directly influence Ly6C expression. Moreover, nidogen-1 and IL-10 were able to reduce Ly6C expression in the absence of IFN-γ (Fig. 6l). Given that IL-10 had the most significant impact on Ly6C expression, we opted to validate its role in vivo to assess the extent by which exogenous Tregs rely on IL-10 expression to promote cardiac repair. CD4$^+$ CD25$^+$ Tregs were isolated from *Il10* knockout mice and administered intravenously one day post-MI (Supplementary Fig. 2c). Compared to saline control, Tregs knocked out for IL-10 (Tregs$^{Il10-/-}$) did not significantly improve cardiac repair outcomes (Fig. 7a–e), suggesting that exogenous Tregs primarily exert their therapeutic effect through IL-10. Collectively, our findings suggest a model in which exogenous Tregs homing to the heart adopt an injury-specific phenotype. This leads to a reduced number of Ly6C^{Hi} CCR2$^+$ Mo/MΦ directly through factors like nidogen-1 and IL-10, and indirectly by reducing CD8$^+$ T cells. Consequently, Mo/MΦ rapidly transition to an anti-inflammatory and pro-repair phenotype, facilitating cardiac repair (Supplementary Fig. 15).

Discussion

MI triggers an intense immune response that significantly influences cardiac repair and adverse remodelling of the infarcted heart[37]. Thus, utilising or controlling the components of the immune system that play an important role in cardiac repair are promising therapeutic strategies[5,6]. Tregs are one of the most important immune regulators, and given their central role in tissue healing, we explored whether a Treg-centric therapeutic strategy would be effective at improving the cardiac repair outcome post-MI. The *Foxp3*$^{DTR/GFP}$ mice was used to confirm that Tregs are critical during cardiac repair. As reported previously, mice depleted of Tregs displayed a worsened cardiac outcome that was characterised by a net increase in infarct size and a reduced ejection fraction[13,16]. Thus, we investigated whether enhancing the number of circulating Tregs in the circulation post-MI through systemic administration of exogenous Tregs would improve cardiac

https://doi.org/10.1038/s41467-024-50806-y

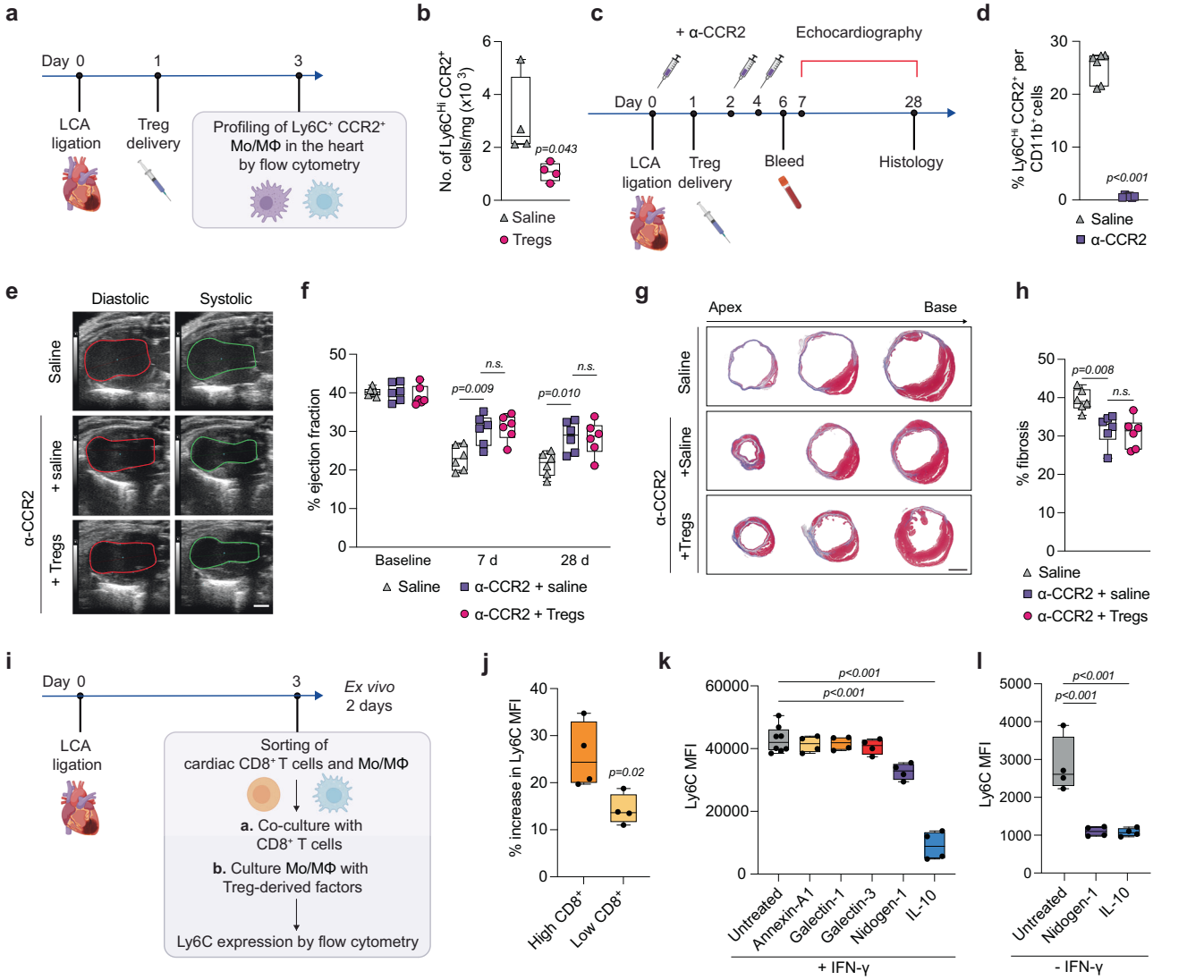

Fig. 6 | Exogenous Tregs decrease the Ly6C^{Hi} CCR2^{+} Mo/MΦ subset in the infarct zone. a, **b** Mice received saline or Tregs 1 day post-MI, and the number of Ly6C^{Hi} CCR2^{+} Mo/MΦ in the infarct zone was assessed by flow cytometry 3 days post-MI. The experimental design is shown in (**a**), and the quantification is presented in (**b**) ($n = 4$). **c**–**h** Mice received anti-CCR2 Fc-silent antibody (α-CCR2) prior treatment along with saline or Tregs one day post-MI. The experimental design is shown in (**c**). **d** Quantification of the Ly6C^{Hi} CCR2^{+} Mo/MΦ in the blood on day 6 post-MI ($n = 6$). **e** Representative parasternal long-axis views of the left ventricle. The red trace is end-diastolic, and the green is end-systolic. **f** Left ventricular ejection fraction measured by echocardiography on baseline, day 7 and day 28 post-MI ($n = 6$). **g** Representative histology of whole transverse heart sections from apex to base stained with Masson's Trichrome staining, 28 days post-MI. Scale bar: 2 mm. **h** Quantification of fibrosis by histology expressed as percentage of the left ventricle ($n = 6$). **i** Experimental design of the ex vivo culture system with sorted cardiac Mo/MΦ and CD8^{+} T cells. Mo/MΦ Ly6C expression was measured by flow cytometry (represented by the geometric mean fluorescence intensity, MFI). **j** Mo/MΦ Ly6C expression expressed as percentage increase relative to high or low numbers of cardiac CD8^{+} T cells ($n = 4$). **k** Mo/MΦ Ly6C expression after stimulation with Treg-derived factors in the presence of IFN-γ ($n = 8$ for untreated, $n = 4$ for exogenous Treg-derived factors). **l** Mo/MΦ Ly6C expression after stimulation with nidogen-1 or IL-10 without IFN-γ ($n = 4$ for untreated, $n = 4$ for exogenous Treg-derived factors). For all graphs, boxes show median (centre line) and interquartile range (edges), whiskers show the range of values and dots represent individual data points. Two-tailed Student's *t*-test was used to compare the groups in (**b**, **d**, **j**). Two-way ANOVA with Bonferroni *post-hoc* test for pair-wise comparisons was used to compare the groups in (**f**). One-way ANOVA with Bonferroni *post-hoc* test for pair-wise comparisons was used to compare the groups in (**k**, **l**). *P*-values are indicated, n.s. indicates non-significant. Panels (**a**, **c**, **i**) created with BioRender.com released under a Creative Commons Attribution-NonCommercial-NoDerivs 4.0 International license (https://creativecommons.org/licenses/by-nc-nd/4.0/deed.en).

repair. To mimic the time course of a treatment that would be administered to a patient suffering from MI, we decided to systemically increase the number of Tregs one day post-LCA ligation, as the first therapeutic interventions usually occur several hours post-MI[38]. In comparison to the saline group, mice that received exogenous Tregs had a significantly improved cardiac repair outcome, as demonstrated by the improved contractility, reduced end-diastolic volume, and reduced fibrosis of the left ventricle. This improved function was observed already one week post-treatment and lasted until the end of the experiment four weeks later, suggesting that the pro-repair effect of Tregs was very rapid and occurred within the first week. The improvement in cardiac functional parameters in response to Treg treatment can be attributed primarily to the significant reduction in cardiomyocyte death. Furthermore, exogenous Tregs may either lead to preservation of existing blood vessels or promote angiogenesis, as indicated by higher vascularisation in the infarcted area compared to saline controls. Our findings are in line with previous studies that demonstrated the therapeutic potential of Tregs to treat MI[10–14,16,39].

https://doi.org/10.1038/s41467-024-50806-y

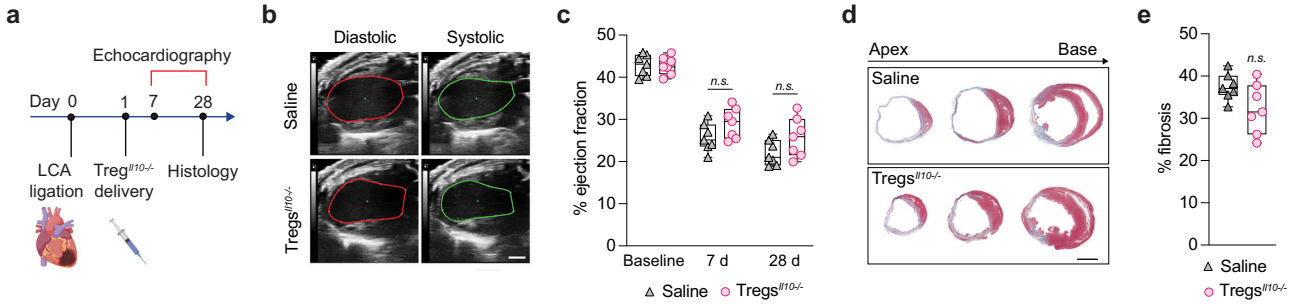

Fig. 7 | Exogenous Tregs primarily exert their therapeutic effect through IL-10. **a**–**e** Mice received saline or Tregs from *Il10* knockout mice (Tregs$^{Il10-/-}$) 1 day post-MI. The experimental design is shown in (**a**). **b** Representative parasternal long-axis views of the left ventricle. The red trace is end-diastolic, and the green is end-systolic. Scale bar: 2 mm. **c** Left ventricular ejection fraction measured by echocardiography 7 and 28 days post-MI ($n = 7$). **d** Representative histology of whole transverse heart sections from apex to base stained with Masson's Trichrome staining, 28 days post-MI. Scale bar: 2 mm. **e** Quantification of fibrosis by histology expressed as percentage of the left ventricle ($n = 7$). For all graphs, boxes show median (centre line) and interquartile range (edges), whiskers show the range of values and dots represent individual data points. Two-way ANOVA with Bonferroni *post-hoc* test for pair-wise comparisons was used to compare the groups in (**c**). Two-tailed Student's *t*-test was used to compare the groups in (**e**). *P*-values are indicated, n.s. indicates non-significant. Panel (**a**) created with BioRender.com released under a Creative Commons Attribution-NonCommercial-NoDerivs 4.0 International license (https://creativecommons.org/licenses/by-nc-nd/4.0/deed.en).

However, the molecular mechanisms by which exogenous Tregs elicit their effect remained elusive.

When determining the pharmacokinetics of exogenous Tregs following delivery, we found that exogenous Tregs quickly home to the heart within the first day following MI, with some Tregs also detected in the spleen and MLN. We did not investigate the mechanisms by which exogenous Tregs home to the infarcted heart, but it is very likely that the inflammatory environment that releases cytokines and chemokines is responsible for the accumulation of exogenous Tregs in the heart[19]. Importantly, we revealed that only the exogenous Tregs which homed to heart underwent a dramatic phenotypic change, while Tregs recovered in the spleen and MLN mostly retained a typical "spleen Treg" phenotype. Indeed, exogenous Tregs recovered from the heart upregulated a series of genes which are also upregulated in endogenous heart Tregs that accumulate much later, and many of those genes are commonly found in Tregs accumulating in other injured tissues[40]. These significant transcriptional changes compared to exogenous Tregs recovered from the spleen indicate that exogenous heart Tregs adapt their phenotype in response to the ischemic microenvironment in a similar way to endogenous heart Tregs.

The amount of exogenous Tregs in the heart decreased one week after delivery, reinforcing the notion that their primary effect is likely concentrated within the first week, aligning with the cardiac function results. A similar decline was observed in the spleen and MLN, suggesting that exogenous Tregs are gradually cleared and/or become diluted in the body when the inflammation triggered by the MI goes down. While exogenous Tregs were effective at promoting cardiac repair, the strategy can likely be optimised. For instance, it was shown that 95% of the Tregs that accumulate in an infarcted heart following MI, come from a pool of circulating Tregs[4]. Thus, we selected to deliver one million cells, because it represents about 5-10 fold the number of Tregs in an adult mouse blood (50,000 to 150,000 Tregs per ml of blood) and about 25–50% of the total number of Tregs[41]. However, delivering a higher number of Tregs or pre-treating Tregs with cytokines to prevent their apoptotic death upon delivery may result in an even better repair[42]. In addition, Treg survival and homing to the heart might be enhanced with pre-amplification and/or pre-treatment of Tregs[43]. While there are no approved Treg-based therapies, GMP-grade Tregs banks exist and Tregs are being explored as adoptive cell therapies to facilitate organ transplantation or for autoimmune diseases[42,44,45]. In those cases, a high number of Tregs and multiple deliveries are required to maintain exogenous Tregs in the body for a long period. However, in the case of MI, Tregs persistence is likely crucial only during the first few days to a week following injury when they modulate the ischemic heart immune microenvironment.

The modulatory effect of endogenous Tregs on Mo/MΦ has been reported in several tissues and organs[46]. For example, mice depleted of Tregs displayed a higher number of inflammatory Mo/MΦ post-MI[13]. Other studies found that the depletion of pro-repair Mo/MΦ results in detrimental cardiac repair outcomes with prolonged inflammation owed by the persistence of pro-inflammatory Mo/MΦ[47,48]. Since we observed that treatment with exogenous Tregs leads to an increase of CD206 expression in cardiac Mo/MΦ at early time points, it suggested that the Tregs rapidly promote Mo/MΦ polarisation towards an anti-inflammatory/pro-repair phenotype. Thus, to determine whether the main mechanism by which exogenous Tregs promote cardiac repair depends on Mo/MΦ, we delivered Tregs in mice that were temporarily depleted of Mo/MΦ with the well-established clodronate liposome method. While Mo/MΦ depletion led to a modest and non-significant reduction in cardiac function, consistent with previous findings in this model[23–25], the therapeutic effect of Tregs was completely abolished in their absence. This experiment demonstrated that exogenous Tregs target Mo/MΦ, either directly or indirectly, to promote cardiac repair post-MI.

RNA sequencing of Mo/MΦ in the infarct zone following Treg administration showed that Mo/MΦ upregulated genes associated to ECM remodelling, macrophage polarisation, and angiogenesis. Amongst upregulated genes in Mo/MΦ at the early time point, we found insulin-like growth factor (*Igf1*) which has been shown to promote angiogenesis as well as cardiomyocyte surivival[49]. In addition, Mo/MΦ upregulated the ECM protein SPARC (osteonectin) at both time points. Interestingly, *Sparc* overexpression has been shown to improve survival by increasing collagen content and enhancing maturation of infarcted area following MI[50]. After one week, Mo/MΦ also upregulated important ECM-related genes including *Dcn* and *Thbs1*. Decorin (*Dcn*) is known to elicit a cardioprotective effect through neutralising and repressing transforming growth factor-β (TGF-β), and when used as a treatment, it reduced the fibrotic scar after MI[51]. Similarly, the ECM protein thrombospondin-1 (*Thbs1*) has been shown to be critical in cardiac repair post-MI. *Thbs1* knockout mice have sustained inflammation comprised of prolonged Mo/MΦ and myofibroblasts infiltration in the heart, which result in an increase in fibrosis via extensive remodelling of the infarcted heart[52]. Along with ECM-related genes, Mo/MΦ upregulated genes characteristics of pro-repair or resident cardiac Mo/MΦ such as *Mrc1*[47], *Csf1r*[48], *Lyve1*[53], *Apoe*[54], *Rbpj*[55], *Cebpb*[56], *Dab2*[57], *Nr4a1*[58], and *Nr4a3*[59]. Interestingly, many of the upregulated ECM-related proteins are also critical for

angiogenesis including, *Sparc*[50], *Dcn*[60], and *Sdc4*[61]. In summary, RNA sequencing of cardiac Mo/MΦ and subsequent validation of the key pro-repair markers CD206 (*Mrc1*), LYVE1, CD163, and SPARC at the protein level in Treg-treated animals revealed that exogenous Tregs influence Mo/MΦ to adopt an anti-inflammatory/pro-repair phenotype. Additionally, they may help preserve cardiac resident macrophages in the remote region of the infarct.

To gain a more comprehensive understanding of the extent to which exogenous Tregs influence Mo/MΦ, we conducted a complementary experiment where we sequenced Mo/MΦ following Treg depletion. RNA sequencing data demonstrated a distinctive shift in the phenotype of cardiac Mo/MΦ towards a pronounced inflammatory state, marked by a significant upregulation of key inflammatory markers such as *Ly6c*, as well as various cytokine and chemokine genes including *Il1b*. Moreover, we noted a significant decrease in the expression of pro-repair genes that were upregulated in response to Treg treatment, including *Thbs1*[52], *Nr4a1*[58], *Lyve1*[53] and *Rbpj*[55]. Notably, the GO terms analysis identified an upregulation in pathways associated with IFN-γ and IL-1 signalling, which are indicative of an intensified inflammatory environment in the absence of Tregs. Concurrently, there was a discernible downregulation in pathways linked to IL-10 production, further emphasising a pro-inflammatory state. As the expression profile of Mo/MΦ following Treg depletion contrasted with their phenotype following Treg treatment, this dataset not only demonstrates the effect of Tregs on Mo/MΦ but also sheds light on the modulation of the Ly6C^{Hi} Mo/MΦ subset by Tregs.

Inflammatory monocytes, characterised by high expression of Ly6C and CCR2, are mobilised to the infarcted cardiac tissue in response to injury through chemokine signals, with CCR2 being the primary chemokine receptor involved in this process[27,62]. Studies have shown that the presence of CCR2^{+} Mo/MΦ exacerbates repair following MI, with their abundance correlating with increased inflammation and diminished cardiac function[63]. In line with these findings, we found that exogenous Tregs led to a significant reduction in the accumulation of the Ly6C^{Hi} CCR2^{+} Mo/MΦ subset in the infarct. Furthermore, blocking the migration of CCR2^{+} Mo/MΦ during the first week post-MI improved the repair outcome, which confirmed the detrimental effect of Ly6C^{Hi} CCR2^{+} Mo/MΦ on cardiac repair. However, the addition of exogenous Tregs in CCR2 depleted mice did not further enhance cardiac repair. Therefore, our results suggest that exogenous Tregs exert their reparative effects by acting on the Ly6C^{Hi} CCR2^{+} Mo/MΦ subset, not only by reducing their accumulation but also by influencing their polarisation in the infarcted heart. Interestingly, when Ly6C^{Hi} CCR2^{+} monocytes accumulate in the heart post-MI, they differentiate into multiple different macrophage subsets characterised by low expression of Ly6C and varying expression levels of CCR2[64]. Moreover, resident macrophages characterised by CCR2^{-} are known to be critical for cardiac repair[63,64]. Indeed, studies have shown that Ly6C^{Hi} monocytes mobilise to the heart and eventually differentiate into anti-inflammatory Mo/MΦ that may contribute to repopulation of the resident Mo/MΦ pool in the heart, accompanied by an increased protein expression of *Mrc1, Lyve1* and *Cd163*[28,29,53]. Given that our study demonstrated an increase in *Lyve1* expression in cardiac Mo/MΦ from Treg-treated animals and its inverse in Treg-depleted animals, it suggests that exogenous Tregs may also influence Mo/MΦ differentiation towards anti-inflammatory/pro-repair resident Mo/MΦs. Nevertheless, further studies will be required to delineate the specific changes to the resident macrophage population in response to exogenous Tregs.

The increase in IFN-γ and IL-1 signalling pathways in cardiac Mo/MΦ following Treg depletion suggest that Mo/MΦ sense a more inflammatory environment in the absence of Tregs. Thus, since we observed a decrease in cytotoxic CD8^{+} T cells in response to exogenous Tregs during the first ten days post-MI, and as CD8^{+} T cells are a major source of IFN-γ[65], we investigated whether the effect of exogenous Tregs on Mo/MΦ was indirectly linked to the reduction of CD8^{+} T cells. The co-culture system demonstrated that a lower number of CD8^{+} T cells directly correlates with a lower level of Ly6C and indicates that CD8^{+} T cells can keep cardiac Mo/MΦ in an inflammatory state. These results align with a previous study demonstrating that depleting CD8^{+} T cells in mice after MI improves cardiac repair, in part due to Mo/MΦ adopting a more pro-repair and less inflammatory profile[66]. Additionally, CD8^{+} T cells were found to directly promote cardiomyocyte death[66]. While our study did not investigate the detailed mechanisms through which exogenous Tregs reduce CD8^{+} T cells in the heart, Tregs are known to control CD8^{+} T cells through multiple mechanisms, including suppressing their proliferation[67].

To test a possible direct effect of exogenous Tregs on Mo/MΦ, we examined if factors highly expressed by exogenous Tregs could reduce Ly6C expression in Mo/MΦ from infarcted hearts using the ex vivo culture system. We selected annexin-A1, galectin-1, galectin-3, nidogen-1, and IL-10, as these factors were expressed in exogenous Tregs recovered from the heart and they have been linked to pro-repair Mo/MΦ polarisation[2,33–36]. For instance, nidogen-1, an ECM basement membrane protein, has been found to elicit a cardioprotective effect by inhibiting the secretion of pro-inflammatory cytokines tumour necrosis factor (TNF)-α and IFN-γ[35]. IL-10 has been shown to improve cardiac function by reducing inflammation and stimulating pro-repair Mo/MΦ polarisation following MI in mice[36,68]. Interestingly, we found that nidogen-1 and IL-10 were able to significantly reduce the Ly6C levelin cardiac Mo/MΦ, indicating that those factors likely directly mediate the effect of exogenous Tregs. Further supporting that IL-10 is critical in Treg-mediated cardiac repair, exogenous Tregs knocked out for IL-10 were not able to significantly improve cardiac repair outcomes post-MI. Nonetheless, the other Treg-derived factors may also contribute to mediating cardiac repair via various mechanisms. For example, annexin-A1 has been shown to promote the production of vascular endothelial growth factor (VEGF)-A from reparative Mo/MΦ, following MI in the mouse[2]. Galectin-1 has been reported to enhance IL-10 production by T cells and decrease survival of CD8^{+} cytotoxic T cells[69]. Similarly, galectin-3 has been shown to promote cardiac repair in mice post-MI by promoting the production of osteopontin from pro-repair CD206^{+} Mo/MΦ[34]. Collectively, our data suggest that exogenous Tregs influence Mo/MΦ directly through factors they express and indirectly by modulating the number of CD8^{+} T cells in the infarcted area.

In conclusion, this study highlights the effectiveness of a Treg-based therapeutic approach for MI where rapid Treg accumulation in the ischemic heart is a crucial factor for improving cardiac repair. Increasing the number of Tregs in the circulation post-MI via systemic delivery of exogenous Tregs greatly enhances cardiomyocyte survival, improves cardiac function, and enhances overall repair outcomes. Mechanistically, we demonstrated that exogenous Tregs rapidly go to the infarct site and have a substantial impact on cytotoxic CD8^{+} T cells and Mo/MΦ, which are key immune cells controlling cardiac repair. Moreover, we revealed that exogenous Tregs homing in the infarcted heart adopt a tissue-injury profile leading to reduced accumulation of Ly6C^{Hi} CCR2^{+} Mo/MΦ and promoting their rapid polarisation toward a pro-repair phenotype. Overall, these findings reveal key mechanisms by which exogenous Tregs influence the immune microenvironment post-MI, particularly in relation to Mo/MΦ phenotype shifts and subsets. These insights into the Treg mechanism of action are directly relevant for the development of Treg-centric therapies for MI, encompassing both immune cell-based approaches and compounds that promote Treg expansion.

Methods

Animals

All animal studies were approved by the Monash Animal Research Ethics committee (15216, 38561) in a specific pathogen–free facility. C57BL/6 J wild-type mice were purchased from the Monash Animal

Research Platform. *Foxp3*$^{IRES\text{-}mRFP}$ mice were bred in house from the Jackson laboratory strain 008374 received from Dr Ajithkumar Vasanthakumar, Olivia Newton-John Cancer Research Institute. *Foxp3*$^{DTR/GFP}$ were bred in house using the Jackson laboratory strain 016958. *Il10*$^{-/-}$ (B6.129P2-*Il10*^{tm1Cgn}/J) mice strain 002251 were purchased from Jackson laboratory. All mice were housed in 12:12 light:-dark light cycles at room temperatures ranging between 20 °C and 24 °C and humidities between 40 and 60%. Food and water were available ad libitum to the mice. Regular diet (BARASTOC) was provided.

Myocardial Infarction model

MI was surgically induced as described previously[70]. Male mice (10-week-old) were anesthetised with isoflurane and attached to an artificial respirator by endotracheal cannulation. The artificial respirator was used to maintain isoflurane concentration at 2% vol/vol with 100% O_2 and operated at a stroke volume of 200 µl at 120 strokes per min. An oblique 8 mm incision was made 2 mm away from the left sternal border toward the left armpit to reveal pectoral muscles. An incision was made through the muscle of the 4th intercostal space. The LCA was visualised as a pulsating bright red spike. Using a micro-needle holder, a 6 mm tapered needle with 8–0 polyethylene suture was passed through the myocardium underneath the LCA, and the ligature was tied with three knots. Occlusion was confirmed by the change of colour of the anterior wall of the left ventricle. Mouse thoracic cavity, and skin incision were closed and sutured. Immediately after surgical procedure, the mice were transferred to a heated pad in a supine position and connected to an artificial respirator pumping air without isoflurane to allow the mice to regain consciousness. Once mice became conscious, the cannula was removed, and the mice were placed on a heating pad for recovery. Subcutaneous buprenorphine analgesia (0.1 mg/kg) was administered for three consecutive days following the surgery as a preventive measure. Animals were monitored by the investigators twice during the first day after surgery and daily for the next nine days. They were assessed for signs of distress, malnutrition, infection, and any other morbidity. Signs of morbidity included abnormal respiration, severe mobility impairment, scruffy coat, abnormal behavior, visible lesions, hunching, and weight loss (more than 10% of total body weight). At any significant sign of distress or at the end of the experiments, animals were euthanized by cervical dislocation or CO_2 asphyxiation.

Sorting endogenous spleen Tregs and systemic Treg delivery

Foxp3$^{DTR/GFP}$ female and male mice were used for sorting of endogenous GFP$^+$ Tregs, *Foxp3*$^{IRES\text{-}mRFP}$ female and male mice for RFP$^+$ Tregs, and *Il10*$^{-/-}$ female mice for CD4$^+$ CD25$^+$ Tregs from the spleen. Cell surface staining was performed according to standard procedures using the following anti-mouse antibodies: APC anti-CD4 (BioLegend, Clone GK1.5, 2 µg/ml); PE/Cyanine7 anti-CD3 (BioLegend, Clone 17A2, 2.7 µg/ml); PE anti-CD25 (Biolegend, Clone PC61, 1 µg/ml). Viability was detected with 1 µg/ml of 4′, 6-diamidino-2-phenylindole dihydrochloride (DAPI). Spleen Treg sort involved a one-step sort process in which CD3$^+$, CD4$^+$, GFP$^+$/RFP$^+$ cells or CD4$^+$, CD25$^+$ cells were sorted. Tregs were sorted on the BD Influx™ cell sorter through a 70 µm nozzle. For all Treg treated groups, 1×10^6 CD4$^+$, GFP$^+$ or CD4$^+$, RFP$^+$ or CD4$^+$, CD25$^+$ Tregs were delivered intravenously in 100 µl RPMI one day post-MI via the lateral tail vein.

Echocardiography

Cardiac ultrasound analysis was performed using Vevo 2100 system (FUJIFILM/VisualSonics, Canada) equipped with a with a 30-MHz linear array transducer (MS550D). On day 1 (baseline), day 7 and day 28 post-MI, the animals were scanned under light anaesthesia (isoflurane in oxygen 1.5 vol%). Hair in the thoracic region was removed using a depilatory cream (Nair), and ultrasound gel was applied to the depilated region. Two-dimensional imaging (B-mode) was performed to obtain parasternal short axis views and long axis views. For long-axis B-mode measurements the endocardium was traced from the atrio-ventricular junction, excluding the papillary muscle. Echocardiographic measurements of the left ventricular ejection fraction, end-diastolic volume, end-systolic internal diameter, anterior wall and posterior wall thickness were calculated using VevoLab software (V3.1.0).

Immunofluorescence and histology

To prepare mouse hearts for paraffin sectioning, hearts were briefly washed in PBS, and fixed in 10% formalin at room temperature. Formalin-fixed tissues were embedded in paraffin and cut into 4 µm tissue sections, de-waxed in xylene for 10 min and rehydrated with alcohols at decreasing concentration (100%, 90%, 70%, 50%) at room temperature. Antigen retrieval was performed on sections by boiling 20 min with 10 mM sodium citrate buffer solution at pH 6.0. All samples were washed three times in PBS, permeabilised in 0.2% Triton 100-X in PBS for 5 min, then washed with PBS-T (PBS with 0.05% tween-20) before blocking in 10% normal goat serum in 1% BSA/PBS for 2 hours. For sections requiring blocking of endogenous IgG, we performed an additional blocking step with an unconjugated affinity purified F(ab) fragment anti-mouse IgG (H + L) (Jackson ImmunoResearch, #AB_2338476) for 1 hour at room temperature. Sections were stained overnight at 4 °C with rabbit anti- mouse CD31 (Abcam, #ab124432, 2 µg/ml); rabbit anti- mouse phospho-histone 3 (pH3) (Abcam, #ab32107, 1 µg/ml); mouse anti- mouse cardiac troponin T (cTnT) (Thermo Fisher Scientific, #13-11, 5 µg/ml); rat anti-mouse CD163 (Abcam, #ab289979, 2 µg/ml) and rabbit anti-mouse F4/80 (Abcam, #ab111101, 1 µg/ml) in 1% normal goat serum in 0.1% BSA/PBS. For cryosectioning, hearts were briefly washed in PBS, and fixed in 4% paraformaldehyde for 4 hours, washed with PBS, cryoprotected overnight in 30% sucrose, and embedded in optimum cutting temperature (O.C.T) compound for cryo-sectioning (10 µm thickness). Sections were stored at −20 °C. Prior processing, sections were briefly thawed at room temperature for 15 min, washed with PBS, and permeabilised with PBS containing 0.2% Triton X-100 for 4 minutes. Blocking was performed with PBS containing 1% bovine serum albumin (BSA) with 10% normal goat serum (NGS) for 1 h at room temperature. Sudan Black B solution (0.1% in 70% ethanol, Sigma, #199664) was applied to tissue sections for 10 minutes to reduce tissue autofluorescence. Sections were stained with primary anti-mouse antibodies: rabbit anti-mouse CD206 (Abcam, #ab64693, 1 µg/ml), rabbit anti-mouse LYVE1 (Abcam, #ab14917, 2 µg/ml), rabbit anti-mouse SPARC (Abcam, #ab290636, 3 µg/ml) and rat anti-mouse F4/80 (Thermo Fisher Scientific, #14-4801-82, 5 µg/ml) were added in in 1% normal goat serum in 0.1% BSA/PBS overnight at 4 °C. After two washing steps of 5 minutes in PBS-T, sections were incubated for 2 h in a secondary antibody: Goat anti-rabbit Alexa Fluor-488 (Thermo Fisher Scientific, #A-11008, 2 µg/ml), Goat anti-rabbit Alexa Fluor-594 (Thermo Fisher Scientific, #A-11012, 2 µg/ml), Goat anti-rat Alexa Fluor-594 (Thermo Fisher Scientific, #A-11012, 2 µg/ml), Goat anti-rat Alexa Fluor-488 (Thermo Fisher Scientific, #A-11006, 2 µg/ml) or Goat anti-mouse Alexa Fluor-647 (Thermo Fisher Scientific, #A-21235, 2 µg/ml) in 1% normal goat serum in 0.1%BSA/PBS at room temperature. Nuclei were stained with 1 µg/ml of DAPI. Masson's trichrome staining was performed to analyse fibrosis. Infarct size was measured as the percentage of the total left ventricular area showing fibrosis. Four µm sections were cut from apex to base and six serial sections at intervals of 350–500 µm were analysed per animal. The mean of the six sections was used to calculate the percentage of fibrosis from the total left ventricular area, using Fiji.

Evaluation of macrophage protein expression

Heart samples were collected on day 7 post-MI from wild-type mice treated with saline or Tregs. Sections were immunostained as detailed

above, imaged on a Leica DMi8 fluorescent microscope, and processed using Fiji. Binary images were created with an optimal threshold and overlapping areas of the protein of interest (CD206, LYVE1, CD163 and SPARC) in F4/80$^+$ cells were determined by combining the binary images. Raw integrated density representing the total pixels was calculated per field of view. The number of F4/80$^+$ cells per field was counted and four fields of view were analysed per heart to calculate the density of the protein of interest/ F4/80$^+$ cells.

TUNEL assay

Myocardial apoptosis was examined using the In Situ Cell Death Detection Kit, TMR red (Roche, #12156792910). Three days post-delivery of the Tregs, formalin-fixed tissues were embedded in paraffin and cut into 4 μm tissue sections, de-waxed in xylene for 10 min and rehydrated with alcohols at decreasing concentration (100%, 90%, 70%, 50%) at room temperature. All samples were washed three times in PBS, permeabilised in 0.2% Triton 100-X in PBS for 8 min. Samples were washed with PBS and 50 μl of the TUNEL reaction mixture from the kit was added on each heart section for 1 h at 37 °C. Slides were washed with HBSS (Hank's Buffered Salt Solution) and incubated with anti-wheat germ agglutinin (WGA) antibody conjugated with FITC (Sigma-Aldrich, # L4895-2MG, 20 μg/ml) for 2 hours at room temperature followed by 1 μg/ml of DAPI. Two slides from each block were evaluated for percentage of apoptotic cells and three fields on each slide were examined at the infarct and border areas. The cardiomyocytes were considered apoptotic if the TUNEL staining was in the middle of a cell with its borders stained by WGA[71]. The number of apoptotic cardiomyocytes is presented as a percentage of total cardiomyocytes.

Treg depletion

Ten-week-old *Foxp3*$^{DTR/GFP}$ and wild-type C57BL/6 J mice received intraperitoneal injections of 20 ng/g diphtheria toxin, starting two days prior to the induction of MI and continuing daily until the day of MI induction, followed by every 2 days after MI, until day 8. Blood from the tail vein was collected on day 7 to confirm Foxp3$^+$ Treg depletion in *Foxp3*$^{DTR/GFP}$ mice.

Mo/MΦ depletion

A total of 7 μl of clodronate liposome (5 mg/ml) solution per gram of mouse was injected intraperitoneally into C57BL6/J mice (body weight 20–30 g) starting one day before injury, on day of surgery and every second day until day 6. Clodronate liposomes were purchased from LIPOSOMA BV (CP-005-005).

Cell isolation from the heart

Hearts were perfused with 5 L/min of HBSS for 5 min immediately after cervical dislocation of the animal. After perfusion, hearts were removed from the chest and chopped in 0.5 mm pieces and transferred in 5 ml of digestion solution (2 mg/ml collagenase II and 100 μg/ml DNase I in 5% heat-inactivated (HI) FBS/HBSS). Digestion was performed at 37 °C for 30 min for two serial digestions. Digestion was terminated by adding RPMI (for T cells) or DMEM/F10 (for Mo/MΦ) containing 10% HI FBS and 10 mM EDTA and passed through a 70 μm filter. Samples were centrifuged for 10 min at 400 x g, and the pellets were resuspended in 5 ml 5% HI FBS and 5 mM EDTA in PBS (FACS buffer).

Flow cytometry

T cells in the heart were stained with the following anti-mouse antibodies for 30 min at 4 °C in 5% HI FBS and 5 mM EDTA in PBS (FACS buffer): APC and BV605 conjugated anti-CD4 (BioLegend, Clone GK1.5, 2 μg/ml); PE/Cyanine7 anti-CD3 (BioLegend, Clone 17A2, 2.7 μg/ml); BV421 anti-CD8 (BioLegend, Clone 53-6.7, 2 μg/ml); PE anti-CD25 (BioLegend, Clone PC61, 2 μg/ml). For intracellular staining, cells are fixed with the eBioscience Fixation/Permeabilization diluent and concentrate (Thermo Fisher Scientific, #00-5223-56, #00-5123-43), then stained with FITC anti-mouse Foxp3 (Tonbo Biosciences, Clone 3G3, 10 μg/ml) in 0.5% saponin for 30 min at 4 °C. If intracellular staining was required, viability was measured by staining the cells with LIVE/DEAD™ Fixable Aqua Dead Cell Stain Kit, for 405 nm excitation (Thermo Fisher Scientific, #L34957, 1:500) prior to surface staining. Otherwise, viability was detected with 1 μg/ml of DAPI or Propidium iodide (PI) (Thermo Fisher Scientific, #P3566). Myeloid cells in the heart were stained with the following anti-mouse antibodies for 30 min at 4 °C in FACS buffer: BV711, PE and APC-Fire750 anti-CD11b (BioLegend, Clone M1/70, 2 μg/ml); PE and BV711 anti-F4/80 (BioLegend, Clone BM8, 8 μg/ml); PE/Cyanine7 anti-CD206 (BioLegend, Clone C068C2, 2 μg/ml); BV421, BV711 and PerCP/Cyanine5.5 anti-Ly6G (BioLegend, Clone 1A8, 2 μg/ml); FITC anti-Ly6C (BioLegend, Clone HK1.4, 6.7 μg/ml); BV421 anti-CCR2 (BioLegend, Clone SA203G11, 2 μg/ml), PerCP/Cyanine5.5 anti-Siglec-F (BioLegend, Clone S17007L, 2 μg/ml); PE/Cyanine7 anti-CD115 (BioLegend, Clone AFS98, 2.7 μg/ml). Viability was detected with 1 μg/ml of DAPI or Propidium iodide (PI). The cells were analysed using the BD Fortessa flow cytometer and the FlowJo application.

Sorting of exogenous Tregs post-delivery

Cell sorting of RFP$^+$ exogenous Tregs: Three days post-MI, each mouse that had been injected with RFP$^+$ Tregs was used to recover the exogenous RFP$^+$ Tregs from the infarcted heart, spleen and MLN. Cell surface staining was performed according to standard procedures using the following anti-mouse antibodies: APC anti-CD4 (BioLegend, Clone GK1.5, 2 μg/ml); PE/Cyanine7 anti-CD3 (BioLegend, Clone 17A2, 2.7 μg/ml); BV711 anti-CD11b (BioLegend, Clone M1/70, 2 μg/ml); BV711 anti-F4/80 (BioLegend, Clone BM8, 8 μg/ml). Viability was detected with 1 μg/ml of DAPI. Tregs were sorted as CD3$^+$, CD11b$^-$, Ly6G$^-$, F4/80$^-$, CD4$^+$, RFP$^+$ cells, on the BD FACSAria™ Fusion flow cytometer (BD Biosciences), through a 70 μm nozzle. Triplicate wells (of 50 cells per well) were sorted for each of the 3 tissues, per individual animal. The cells were directly sorted into a chilled 384-well PCR plate (Greiner, 785290), containing 1.2 μL of primer/lysis mix in each well [20 nM indexed polydT primer (custom made, IDT), 1:6.000.000 dilution of ERCC RNA spike-in mix (Ambion – 4456740), 1 mM dNTPs (NEB–N0446S), 1.2 units SUPERaseIN Rnase Inhibitor (Thermo Fisher Scientific- AM2696), 0.2 % Triton X-100 solution (Sigma Aldrich – 93443-100 ml), DEPC water (Thermo Fisher Scientific- AM9920)]. Sorted plates were sealed, centrifuged for 1 min at 3000 rpm and immediately frozen upside down at −80 °C until further processing for mini-bulk RNA sequencing.

Sorting of cardiac Mo/MΦ

Cell surface staining was performed according to standard procedures using the following anti-mouse antibodies: PerCP/Cyanine5.5 anti–Siglec-F (BioLegend, Clone S17007L, 2 μg/ml); PerCP/Cyanine5.5 anti-Ly6G (BioLegend, Clone 1A8, 2 μg/ml); APC-Fire750 anti-CD11b (BioLegend, Clone M1/70, 2 μg/ml); PE anti-F4/80 (BioLegend, Clone BM8, 8 μg/ml). Viability was detected with 1 μg/ml of DAPI. Mo/MΦ were sorted on the BD Influx™ cell sorter through a 100 μm nozzle.

Sorting of endogenous heart Tregs

GFP$^+$ endogenous heart Tregs were sorted from the infarcted hearts of *Foxp3*$^{DTR/GFP}$ mice one week post-MI. Cell surface staining was performed according to standard procedures using the following anti-mouse antibodies: APC anti-CD4 (BioLegend, Clone GK1.5, 2 μg/ml); PE/Cyanine7 anti-CD3 (BioLegend, Clone 17A2, 2.7 μg/ml); BV711 anti-F4/80 (BioLegend, Clone BM8, 8 μg/ml). Viability was detected with 1 μg/ml of DAPI. Endogenous heart Tregs were sorted using a two-step process that included enrichment of CD3$^+$, CD11b$^-$, F4/80$^-$ cells and purity sort of CD4$^+$, GFP$^+$ cells. Tregs were sorted on the BD Influx™ cell sorter through a 100 μm nozzle.

RNA isolation

Total RNA was isolated from the sorted endogenous Mo/MΦ and endogenous Tregs (from uninjured spleen and infarcted heart) using the RNeasy Plus Micro Kit (Qiagen, #74034) according to the manufacturer's instructions. RNA concentration was measured using a Qubit Fluorometer (Invitrogen) and RNA quality was assessed using the Bioanalyzer 2100 system (Agilent Technologies).

Mini-bulk RNA sequencing of exogenous Tregs and endogenous Mo/MΦ

Mini-bulk RNA sequencing was performed using a modified CEL-Seq2 protocol[26], which allowed us to perform RNA sequencing with limited numbers of cells obtained after sorting recovered (exogenous) Tregs from the heart, spleen and MLN of each mouse. For consistency, the same technique was used to perform RNA-seq on Mo/MΦ sorted from the infarcted heart after Treg treatment (wherein we sorted cells from one mouse heart per biological replicate and extracted RNA from each biological replicate for RNA-seq). For the recovered exogenous Tregs, mini-bulk RNA-sequencing was performed on 27 wells of sorted samples in a 384-well plate (3 tissues from 3 individual animals, each sorted as 3 technical replicates), containing 50 cells/well. For the endogenous Mo/MΦ from infarcted heart tissue, 1.1 µl of purified Mo/MΦ RNA (6 ng/ µl) from each sample was added to a well of a 384-well PCR plate (Greiner, 785290) containing 20 nM of an air dried indexed polydT primer (custom made, IDT). First strand cDNA synthesis was performed by using a reverse transcription reaction mix (Invitrogen − 18064-014) according to the manufacturer's instructions. The recovered Treg samples were then pooled into 1.5 ml Eppendorf LoBind microcentrifuge tubes, while the individual Mo/MΦ samples were transferred separately to other 1.5 ml tubes. These samples were then treated with Exonuclease I [NEB−M0293L; 20 U/µl] for 30 minutes at 37 °C, followed by 80 °C for 10 minutes, followed by a 1.2 X bead clean-up. The eluted cDNA was then used for second strand synthesis performed with the NEBNext Second Strand Synthesis module (NEB #E6111S) in a final reaction volume of 20 µl to generate double stranded cDNA followed by a 1.2X bead clean-up. All DNA purification and size selection steps were done using the NucleoMag NGS Clean-up and Size select magnetic beads (Macherey-Nagel − 7449970.5), according to manufacturer's instructions. In vitro transcription (IVT) was then performed on the eluted cDNA using the T7 enzyme (MEGAscript T7 Transcription Kit−Ambion AM1334) incubated at 37 °C for 13 h, after which left-over primers were removed using the ExoSAP-IT For PCR Product Clean-Up kit (Affymetrix −78200). The sample was then subjected to RNA fragmentation by chemical heat incubation with RNA fragmentation reagents−Ambion AM8740) and subsequent purification using 1.8X RNAClean XP beads (Beckman coulter−A63987) according to the manufacturer's instructions. The fragmented RNA was transcribed into cDNA using 5′-tagged random hexamer primers (GCCTTGGCACCCGAGAATTCCANNNNNN) introducing a partial Illumina adapter as also described in the CEL-Seq2 protocol[26] to perform the 5′-tagged-random-hexamer reverse transcription (ranhexRT). PCR was performed using half of the ranhexRT sample as a template [1X KAPA HiFi HotStart ReadyMix (KapaBiosystems KK2602), 400 nM each primer]. Then the final PCR-amplified library was submitted to two consecutive 1X bead clean-up steps and then used for sequencing on the Illumina NextSeq2000 instrument (50 cycle kit) including 5% PhiX in the sequencing run.

Analysis of mini-bulk RNA sequencing data

Mini-bulk reads for both sequencing experiments were mapped to the *Mus musculus* GRCm38.p6 genome and ERCC spike-in sequences using the Subread aligner (v2.10.5)[72] and assigned to genes using scPipe (v1.18.0)[73] with GENCODE M25 primary assembly annotation. Gene-based annotations were obtained from the 'EnsDb.Mmusculus.v79' R/Bioconductor package[74], which was used to map the GENCODE/Ensembl gene IDs to gene symbols and to other info (e.g., gene biotype, chromosome location). Gene counts were exported as a matrix by scPipe with UMI-aware counting. For the Treg samples, technical replicates were aggregated by summing the UMI counts, to generate pseudobulked data containing three biological replicates for each of the three tissues (spleen, MLN and heart). The UMI-deduplicated read count files containing this Treg pseudobulked data (combining all technical replicates for each sample into one) was uploaded to Degust web tool[75] for further processing. For the endogenous Mo/MΦ samples, since there were no technical replicates, the original UMI-deduplicated read count files were uploaded to Degust. Degust performs normalisation using trimmed mean of M values (TMM)[76], and differential gene expression analysis using limma/voom[77]. Genes with a false-discovery rate (FDR) < 0.05 were considered significantly differentially expressed (DE). The heat map was generated using the pheatmap function from the pheatmap package (version 1.0.12)[78], along with the RColorBrewer package (version 1.1-3)[79] in R (version 4.2.2). Functional enrichment analysis for GO Biological Processes was performed for the differentially up-regulated genes for Tregs, or up-regulated and down-regulated genes for macrophages, using enrichGO function from the clusterProfiler package (version 3.0.4), and the Benjamini-Hochberg FDR method for multiple testing correction, with the significance threshold of q-value (adjusted p-value) < 0.01) using a minimum gene set size of 4 and maximum of 100. Gene-concept network plots were made using the cnetplot function under the Enrichplot package (version 1.22.0)[80] and the ClusterProfiler package (version 3.0.4)[81] to visualise the network of differentially expressed genes contributing to each GO biological process term.

Bulk RNA sequencing

Bulk RNA sequencing was performed for endogenous heart Tregs and healthy spleen controls, as well as for Mo/MΦ from Treg-depleted mice. For Tregs, RNA quantity/quality assessment, library preparation and sequencing were performed at the Medical Genomics Facility, Monash Health Translation Precinct (MHTP) and at Micromon Genomics (Monash University). Libraries were constructed using the Tecan/Nugen Ovation Solo Library prep kit, starting with 1 ng of input total RNA. Libraries were quantified and quality assessed by Qubit, Bioanalyser and qPCR, and one equimolar pool was prepared based upon size-corrected qPCR quantitation. This library pool was loaded for on-board denaturation and clustering into one lane of the Illumina NextSeq 2000 platform for sequencing (at MHTP) and into one lane of the MGITech MGISEQ2000RS hardware (at Micromon), to generate 100 bp paired-end reads, with a depth of minimum 30 million reads per sample. For Mo/MΦ, RNA quantity/quality assessment, library preparation and sequencing were performed at MHTP. Libraries were constructed starting with 20 ng of input total RNA. Individual first strand synthesis was performed to add the Illumina P7 primer containing an 8 bp sample index and 10 bp unique molecular identifier (UMI) and standard i7/R2 primer during the initial polyA priming. Samples were processed as 3 pools which were amplified using P7 and a template switching oligonucleotide that had been added to the 5′ end of RNA. Three different i5 indexes were used to distinguish the 3 sample pools. The Illumina P5 was added by tagmentation by Nextera transposase during amplification. Libraries were quantified and quality assessed by Qubit, Bioanalyser and qPCR, and one equimolar pool was prepared based upon size-corrected qPCR quantitation. This library pool was loaded for on-board denaturation and clustering into one lane of the Illumina NextSeq 2000 platform for sequencing (at MHTP) using the P3 cycle kit, to generate 60 bp single-end 3′ end reads, with a depth of minimum 15 million reads per sample, or into one lane of the MGITech MGISEQ2000RS hardware (Micromon, Monash University), to generate 100 bp paired-end reads, with a depth of minimum 30 million reads per sample.

Analysis of bulk RNA sequencing data

The sequenced raw FASTQ files for the endogenous Tregs were analysed with the RNASik pipeline[82] using STAR aligner[83] with *Mus musculus* GRCm38 reference. For the macrophages, the analysis was performed using the nfcore/rnaseq 3.3 pipeline (forward-stranded), using STAR aligner[83] with the *Mus musculus* GRCm39 reference, including "with_umi" flag for UMI-deduplication. Reads were quantified using featureCounts[84] producing the raw genes count matrix and various quality control metrics. Raw counts (forward stranded reads) were then analysed with Degust web tool[75] which performs normalisation using trimmed mean of M values (TMM)[76] and differential expression analysis using limma/voom[77]. Samples were batched corrected to account for variation between two different sequencing facilities across replicates. This was done within Degust by adding a covariate to the linear model for each sequencing batch which reduced the noise and improved the power of the test. Genes with a false-discovery rate (FDR) < 0.05 were considered significantly differentially expressed (DE). The MA-plot was generated using GGPlot2[85] in R (version 4.2.2).

CCR2$^+$ cell depletion

To systemically deplete CCR2$^+$ cells, we used anti-CCR2 monoclonal antibody, Mouse IgG2a, Fc Silent, clone MC21 (Absolute Antibody, Ab02444-2.3), as has been previously established[30]. Mice were injected with 20 µg anti-CCR2 antibody intraperitoneally on the day of surgery, as well as on days 2 and 4 post-surgery. Blood from the tail vein was collected on day 6 to confirm CCR2$^+$ systemic depletion.

Ex vivo culture of cardiac Mo/MΦ and CD8$^+$ T cells isolated post-MI

Mo/MΦ and CD8$^+$ T cells were sorted from infarcted hearts on day 3 post-MI, and were centrifuged at 500 x g for 10 min at 4 °C. Both cell types were resuspended in an appropriate volume of RPMI 1640 plus 5% heat-inactivated FBS, with 100 units/ml penicillin/ streptomycin and recombinant mouse M-CSF (10 ng/ml, R&D Systems, #416-ML) for subsequent seeding. For CD8$^+$ T cell and Mo/MΦ co-culture, 10,000 Mo/MΦ were added to ultra-low binding 96-well plates (Sigma-Aldrich), along with either no CD8$^+$ T cells, or with 1000 (low), or 2,000 (high) CD8$^+$ T cells, representing a CD8$^+$ T cells:Mo/MΦ ratio of 1:10 and 1:5, respectively. The suspension of CD8$^+$ T cells and Mo/MΦ was cultured at 37 °C with 5% CO_2 for 48 h before collecting them for subsequent staining steps. For the Treg-derived factors, 20,000 Mo/MΦ were added per well of a 96 well plate, with or without interferon IFN-γ (0.1 ng/ml, Sino Biological, #50709-MNAH), in the presence of Recombinant Mouse annexin-A1 (50 ng/ml, Abcam, #ab202184), Recombinant Mouse galectin-1 (50 ng/ml, R&D Systems, #1245-GA), Recombinant Mouse galectin-3 (50 ng/ml, R&D Systems, #1197-GA), Recombinant Human nidogen-1 (50 ng/ml, R&D Systems, #2570-ND), or Recombinant Mouse IL-10 (10 ng/ml, R&D Systems, #417-ML) treatment. The cells were cultured at 37 °C with 5% CO_2 for 48 h before detaching them with TrypLE (Thermo Fisher Scientific) containing 3 mM EDTA before collecting them for subsequent staining steps.

Statistical analysis

Statistical analyses were performed using GraphPad Prism 9 statistical software (GraphPad, USA). Significant differences were calculated with Student's *t*-test for pairwise comparisons, or by analysis of variance (ANOVA) for three or more groups, followed by Bonferroni *post hoc* test when performing multiple comparisons between groups. $p < 0.05$ was considered statistically significant. The *P* values are indicated and n.s. indicates not significant.

Reporting summary

Further information on research design is available in the Nature Portfolio Reporting Summary linked to this article.

Data availability

All data associated with this study are present in the main text or the supplementary materials. Source data are provided with this paper. All RNA sequencing data presented were generated for this study and have been deposited in NCBI's Gene Expression Omnibus (GEO) database under accession code GSE228871 for bulk RNA-seq of endogenous Tregs, GSE230173 for mini-bulk RNA-seq of macrophages from Treg-treated mice, GSE230177 for mini-bulk RNA-seq of recovered exogenous Tregs and GSE268828 for bulk RNA-seq of macrophages from Treg-depleted mice. Source data are provided with this paper.

References

1. Talman, V. & Ruskoaho, H. Cardiac fibrosis in myocardial infarction-from repair and remodeling to regeneration. *Cell tissue Res.* **365**, 563–581 (2016).
2. Ferraro, B. et al. Pro-Angiogenic Macrophage Phenotype to Promote Myocardial Repair. *J. Am. Coll. Cardiol.* **73**, 2990 (2019).
3. Zhang, R. et al. Bone marrow mesenchymal stem cells transfer in patients with ST-segment elevation myocardial infarction: single-blind, multicenter, randomized controlled trial. *Stem Cell Res Ther.* **12**, 33 (2021).
4. Xia, N. et al. A Unique Population of Regulatory T Cells in Heart Potentiates Cardiac Protection From Myocardial Infarction. *Circulation* **142**, 1956–1973 (2020).
5. Farache Trajano, L. & Smart, N. Immunomodulation for optimal cardiac regeneration: insights from comparative analyses. *NPJ Regen. Med.* **6**, 8 (2021).
6. Rurik, J. G., Aghajanian, H. & Epstein, J. A. Immune Cells and Immunotherapy for Cardiac Injury and Repair. *Circ. Res.* **128**, 1766–1779 (2021).
7. Simoes, F. C. & Riley, P. R. Immune cells in cardiac repair and regeneration. *Development* **149**, dev199906 (2022).
8. Yap, J. et al. Macrophages in cardiac remodelling after myocardial infarction. *Nat. Rev. Cardiol.* **20**, 373–385 (2023).
9. Ilatovskaya, D. V. et al. CD8(+) T-cells negatively regulate inflammation post-myocardial infarction. *Am. J. Physiol. Heart Circ. Physiol.* **317**, H581–H596 (2019).
10. Matsumoto, K. et al. Regulatory T Lymphocytes Attenuate Myocardial Infarction-Induced Ventricular Remodeling in Mice. *Int. Heart J.* **52**, 382–387 (2011).
11. Sharir, R. et al. Experimental Myocardial Infarction Induces Altered Regulatory T Cell Hemostasis, and Adoptive Transfer Attenuates Subsequent Remodeling. *PLoS One* **9**, e113653 (2014).
12. Tang, T.-T. et al. Regulatory T cells ameliorate cardiac remodeling after myocardial infarction. *Basic Res. Cardiol.* **107**, 232 (2011).
13. Weirather, J. et al. Foxp3+ CD4+ T cells improve healing after myocardial infarction by modulating monocyte/macrophage differentiation. *Circ. Res.* **115**, 55–67 (2014).
14. Kvakan, H. et al. Regulatory T Cells Ameliorate Angiotensin II–Induced Cardiac Damage. *Circulation* **119**, 2904–2912 (2009).
15. Saxena, A. et al. Regulatory T cells are recruited in the infarcted mouse myocardium and may modulate fibroblast phenotype and function. *Am. J. Physiol.-Heart Circulatory Physiol.* **307**, H1233–H1242 (2014).
16. Zacchigna, S. et al. Paracrine effect of regulatory T cells promotes cardiomyocyte proliferation during pregnancy and after myocardial infarction. *Nat. Commun.* **9**, 2432 (2018).
17. Zeng, Z. et al. Interleukin-2/Anti-Interleukin-2 Immune Complex Attenuates Cardiac Remodeling after Myocardial Infarction through Expansion of Regulatory T Cells. *J. Immunol. Res.* **2016**, 8493767 (2016).
18. Zhao Tian, X. et al. Regulatory T-Cell Response to Low-Dose Interleukin-2 in Ischemic Heart Disease. *NEJM Evid.* **1**, EVIDoa2100009 (2022).

19. Li, J., Tan, J., Martino, M. M. & Lui, K. O. Regulatory T-Cells: Potential Regulator of Tissue Repair and Regeneration. *Front. Immunol.* **9**, 585 (2018).
20. Koizumi, S.-i et al. JunB regulates homeostasis and suppressive functions of effector regulatory T cells. *Nat. Commun.* **9**, 5344 (2018).
21. Fassett, M. S., Jiang, W., D'Alise, A. M., Mathis, D. & Benoist, C. Nuclear receptor Nr4a1 modulates both regulatory T-cell (Treg) differentiation and clonal deletion. *Proc. Natl Acad. Sci.* **109**, 3891–3896 (2012).
22. Sekiya, T. et al. The nuclear orphan receptor Nr4a2 induces Foxp3 and regulates differentiation of CD4+ T cells. *Nat. Commun.* **2**, 269 (2011).
23. Hess, A., Borchert, T., Ross, T. L., Bengel, F. M. & Thackeray, J. T. Characterizing the transition from immune response to tissue repair after myocardial infarction by multiparametric imaging. *Basic Res. Cardiol.* **117**, 14 (2022).
24. Zhao, E., Xie, H. & Zhang, Y. Predicting Diagnostic Gene Biomarkers Associated With Immune Infiltration in Patients With Acute Myocardial Infarction. *Front. Cardiovasc. Med.* **7**, 586871 (2020).
25. Wang, F. et al. PCSK9 Modulates Macrophage Polarization-Mediated Ventricular Remodeling after Myocardial Infarction. *J. Immunol. Res.* **2022**, 7685796 (2022).
26. Hashimshony, T. et al. CEL-Seq2: sensitive highly-multiplexed single-cell RNA-Seq. *Genome Biol.* **17**, 77 (2016).
27. Dutta, P. & Nahrendorf, M. Monocytes in Myocardial Infarction. *Arteriosclerosis, Thrombosis, Vasc. Biol.* **35**, 1066–1070 (2015).
28. Epelman, S. et al. Embryonic and Adult-Derived Resident Cardiac Macrophages Are Maintained through Distinct Mechanisms at Steady State and during Inflammation. *Immunity* **40**, 91–104 (2014).
29. Dick, S. A. et al. Self-renewing resident cardiac macrophages limit adverse remodeling following myocardial infarction. *Nat. Immunol.* **20**, 29–39 (2019).
30. Mack, M. et al. Expression and Characterization of the Chemokine Receptors CCR2 and CCR5 in Mice1. *J. Immunol.* **166**, 4697–4704 (2001).
31. Patel, B. et al. CCR2+ Monocyte-Derived Infiltrating Macrophages Are Required for Adverse Cardiac Remodeling During Pressure Overload. *JACC: Basic Transl. Sci.* **3**, 230–244 (2018).
32. Saunders, K. O. Conceptual Approaches to Modulating Antibody Effector Functions and Circulation Half-Life. *Front. Immunol.* **10**, 1296 (2019).
33. Abebayehu, D. et al. Galectin-1 promotes an M2 macrophage response to polydioxanone scaffolds. *J. Biomed. Mater. Res. A* **105**, 2562–2571 (2017).
34. Shirakawa, K. et al. IL (Interleukin)–10–STAT3–Galectin-3 Axis Is Essential for Osteopontin-Producing Reparative Macrophage Polarization After Myocardial Infarction. *Circulation* **138**, 2021–2035 (2018).
35. Zbinden, A. et al. Nidogen-1 Mitigates Ischemia and Promotes Tissue Survival and Regeneration. *Adv. Sci.* **8**, 2002500 (2021).
36. Jung, M. et al. IL-10 improves cardiac remodeling after myocardial infarction by stimulating M2 macrophage polarization and fibroblast activation. *Basic Res. Cardiol.* **112**, 33 (2017).
37. Frangogiannis, N. G. The inflammatory response in myocardial injury, repair, and remodelling. *Nat. Rev. Cardiol.* **11**, 255–265 (2014).
38. Vogel, B. et al. ST-segment elevation myocardial infarction. *Nat. Rev. Dis. Prim.* **5**, 39 (2019).
39. Zhuang, R. et al. CD4+FoxP3+CD73+ regulatory T cell promotes cardiac healing post-myocardial infarction. *Theranostics* **12**, 2707–2721 (2022).
40. Miragaia, R. J. et al. Single-Cell Transcriptomics of Regulatory T Cells Reveals Trajectories of Tissue Adaptation. *Immunity* **50**, 493–504.e497 (2019).
41. Wei, S., Kryczek, I. & Zou, W. Regulatory T-cell compartmentalization and trafficking. *Blood* **108**, 426–431 (2006).
42. Raffin, C., Vo, L. T. & Bluestone, J. A. T(reg) cell-based therapies: challenges and perspectives. *Nat. Rev. Immunol.* **20**, 158–172 (2020).
43. Bittner, S. et al. Biosensors for inflammation as a strategy to engineer regulatory T cells for cell therapy. *Proc. Natl Acad. Sci. USA* **119**, e2208436119 (2022).
44. Terry, L. V. & Oo, Y. H. The Next Frontier of Regulatory T Cells: Promising Immunotherapy for Autoimmune Diseases and Organ Transplantations. *Front Immunol.* **11**, 565518 (2020).
45. Qu, G. et al. Current status and perspectives of regulatory T cell-based therapy. *J. Genet Genomics* **49**, 599–611 (2022).
46. Alshoubaki, Y. K., Nayer, B., Das, S. & Martino, M. M. Modulation of the Activity of Stem and Progenitor Cells by Immune Cells. *Stem Cells Transl. Med.* **11**, 248–258 (2022).
47. Shiraishi, M. et al. Alternatively activated macrophages determine repair of the infarcted adult murine heart. *J. Clin. Investig.* **126**, 2151–2166 (2016).
48. Leblond, A.-L. et al. Systemic and Cardiac Depletion of M2 Macrophage through CSF-1R Signaling Inhibition Alters Cardiac Function Post Myocardial Infarction. *PLoS One* **10**, e0137515 (2015).
49. Foncea, R. et al. Extracellular Regulated Kinase, but Not Protein Kinase C, Is an Antiapoptotic Signal of Insulin-like Growth Factor-1 on Cultured Cardiac Myocytes. *Biochem. Biophys. Res. Commun.* **273**, 736–744 (2000).
50. Rienks, M. et al. SPARC preserves endothelial glycocalyx integrity, and protects against adverse cardiac inflammation and injury during viral myocarditis. *Matrix Biol.* **74**, 21–34 (2018).
51. Sylakowski, K. et al. The matricellular protein decorin delivered intradermally with coacervate improves wound resolution in the CXCR3-deficient mouse model of hypertrophic scarring. *Wound Repair Regen.* **30**, 436–447 (2022).
52. Frangogiannis, N. G. et al. Critical Role of Endogenous Thrombospondin-1 in Preventing Expansion of Healing Myocardial Infarcts. *Circulation* **111**, 2935–2942 (2005).
53. Revelo, X. S. et al. Cardiac Resident Macrophages Prevent Fibrosis and Stimulate Angiogenesis. *Circ. Res.* **129**, 1086–1101 (2021).
54. Baitsch, D. et al. Apolipoprotein E Induces Antiinflammatory Phenotype in Macrophages. *Arteriosclerosis, Thrombosis, Vasc. Biol.* **31**, 1160–1168 (2011).
55. Foldi, J., Shang, Y., Zhao, B., Ivashkiv, L. B. & Hu, X. RBP-J is required for M2 macrophage polarization in response to chitin and mediates expression of a subset of M2 genes. *Protein Cell* **7**, 201–209 (2016).
56. Ruffell, D. et al. A CREB-C/EBPβ cascade induces M2 macrophage-specific gene expression and promotes muscle injury repair. *Proc. Natl Acad. Sci.* **106**, 17475–17480 (2009).
57. Adamson, S. E. et al. Disabled homolog 2 controls macrophage phenotypic polarization and adipose tissue inflammation. *J. Clin. Investig.* **126**, 1311–1322 (2016).
58. Hilgendorf, I. et al. Ly-6Chigh Monocytes Depend on Nr4a1 to Balance Both Inflammatory and Reparative Phases in the Infarcted Myocardium. *Circ. Res.* **114**, 1611–1622 (2014).
59. De Paoli, F. et al. The neuron-derived orphan receptor 1 (NOR1) is induced upon human alternative macrophage polarization and stimulates the expression of markers of the M2 phenotype. *Atherosclerosis* **241**, 18–26 (2015).
60. Lai, J. et al. Overexpression of decorin promoted angiogenesis in diabetic cardiomyopathy via IGF1R-AKT-VEGF signaling. *Sci. Rep.* **7**, 44473 (2017).
61. De Rossi, G. et al. Pathological Angiogenesis Requires Syndecan-4 for Efficient VEGFA-Induced VE-Cadherin Internalization. *Arteriosclerosis, Thrombosis, Vasc. Biol.* **41**, 1374–1389 (2021).
62. Bajpai, G. et al. The human heart contains distinct macrophage subsets with divergent origins and functions. *Nat. Med.* **24**, 1234–1245 (2018).
63. Bajpai, G. et al. Tissue Resident CCR2– and CCR2+ Cardiac Macrophages Differentially Orchestrate Monocyte Recruitment and Fate

Specification Following Myocardial Injury. *Circulation Res.* **124**, 263–278 (2019).
64. Chen, B., Brickshawana, A. & Frangogiannis, N. G. The Functional Heterogeneity of Resident Cardiac Macrophages in Myocardial Injury. *Circulation Res.* **124**, 183–185 (2019).
65. Bhat, P., Leggatt, G., Waterhouse, N. & Frazer, I. H. Interferon-γ derived from cytotoxic lymphocytes directly enhances their motility and cytotoxicity. *Cell Death Dis.* **8**, e2836 (2017).
66. Santos-Zas, I. et al. Cytotoxic CD8+ T cells promote granzyme B-dependent adverse post-ischemic cardiac remodeling. *Nat. Commun.* **12**, 1483 (2021).
67. Chen, M.-L. et al. Regulatory T cells suppress tumor-specific CD8 T cell cytotoxicity through TGF-β signals in vivo. *Proc. Natl Acad. Sci.* **102**, 419–424 (2005).
68. Krishnamurthy, P. et al. IL-10 Inhibits Inflammation and Attenuates Left Ventricular Remodeling After Myocardial Infarction via Activation of STAT3 and Suppression of HuR. *Circulation Res.* **104**, e9–e18 (2009).
69. Cedeno-Laurent, F., Opperman, M., Barthel, S. R., Kuchroo, V. K. & Dimitroff, C. J. Galectin-1 triggers an immunoregulatory signature in Th cells functionally defined by IL-10 expression. *J. Immunol.* **188**, 3127–3137 (2012).
70. Muthuramu, I., Lox, M., Jacobs, F. & De Geest, B. Permanent ligation of the left anterior descending coronary artery in mice: a model of post-myocardial infarction remodelling and heart failure. *J. Visualized Exp.: JoVE.* **94**, e52206 (2014).
71. Le, T. Y. L., Ogawa, M., Kizana, E., Gunton, J. E. & Chong, J. J. H. Vitamin D improves cardiac function after myocardial infarction through modulation of resident cardiac progenitor cells. *Heart, Lung Circulation.* **27**, 967–975 (2018).
72. Liao, Y., Smyth, G. K. & Shi, W. The Subread aligner: fast, accurate and scalable read mapping by seed-and-vote. *Nucleic Acids Res.* **41**, e108–e108 (2013).
73. Tian, L. et al. scPipe: A flexible R/Bioconductor preprocessing pipeline for single-cell RNA-sequencing data. *PLOS Comput. Biol.* **14**, e1006361 (2018).
74. Rainer J. Ensembl based annotation package. In: *EnsDb.Mmusculus.v79*) (2017).
75. David R. Powell A. P., Michael Milton. Degust: Interactive Rna-Seq Analysis.) (2019).
76. Robinson, M. D. & Oshlack, A. A scaling normalization method for differential expression analysis of RNA-seq data. *Genome Biol.* **11**, R25 (2010).
77. Law, C. W., Chen, Y., Shi, W. & Smyth, G. K. voom: Precision weights unlock linear model analysis tools for RNA-seq read counts. *Genome Biol.* **15**, R29 (2014).
78. Kolde R. pheatmap: Pretty Heatmaps. *R package version 1012*, (2019).
79. Neuwirth E. RColorBrewer: ColorBrewer Palettes. *R package version 11-3*, (2022).
80. Yu G. enrichplot: Visualization of Functional Enrichment Result. *R package version 1200*, (2023).
81. Wu, T. et al. clusterProfiler 4.0: A universal enrichment tool for interpreting omics data. *Innov. (Camb.)* **2**, 100141 (2021).
82. Tsyganov, K., Perry, A., Archer, S. K. & Powell, D. RNAdsik: A Pipeline for complete and reproducible RNA-seq analysis that runs anywhere with speed and ease. *J. Open Source Softw.* **3**, 28 (2018).
83. Dobin, A. et al. STAR: ultrafast universal RNA-seq aligner. *Bioinformatics* **29**, 15–21 (2013).
84. Liao, Y., Smyth, G. K. & Shi, W. featureCounts: an efficient general purpose program for assigning sequence reads to genomic features. *Bioinformatics* **30**, 923–930 (2014).
85. Wickham H. ggplot2: Elegant Graphics for Data Analysis.). Springer-Verlag New York (2016).

Acknowledgements

We thank the Monash Animal Research Platform, Monash Micro Imaging Platform and Monash Biomedical Imaging. We acknowledge the use of equipment and technical assistance of the Monash Histology Platform, Department of Anatomy and Developmental Biology, Monash University. We acknowledge Dr. Michael de Veer at Monash Biomedical Imaging for his support with the echocardiography experiments, Dr. Trevor Wilson at the MHTP Medical Genomics Facility for bulk RNA sequencing, Dr. Casey J.A. Anttila and Dr. Tracey M. Baldwin from The Walter and Eliza Hall Institute Flow Cytometry Facility and Advanced Genomics Facility for flow cytometry and experiment design of mini-bulk RNA sequencing, the Monash Bioinformatics Platform (Prof. David Powell, Dr. Deanna Deveson Lucas, Dr. Andrew Perry and Ms. Adele Barugahare) for assistance with processing and analysis of RNA sequencing data, Dr. Ziad Julier for his help with intravenous injections, Mr. Anthony Park for his help with animal colonies, Dr. Alon M. Douek for his help with the TUNEL assay, microscopy and bioinformatics advice, and Ms. Monika Mohenska for bioinformatics support. Biorender.com was used to create some illustrations in the figures. This work was partially funded by the National Health and Medical Research Council (APP1140229 and APP1176213), the Medical Research Future Fund (APP1202105), the Viertel Charitable Foundation Senior Medical Researcher Fellowship to M.M.M., and by the Heart Foundation of Australia Future Leader Fellowship (102036) to G. dM.-N. The Australian Regenerative Medicine Institute is supported by grants from the State Government of Victoria and the Australian Government.

Author contributions

Y.K.A. and M.M.M. conceptualised the study. Y.K.A., B.N., and M.M.M. designed the experiments. Y.K.A. conducted majority of all experiments and data analysis. B.N. helped with all mechanistic experiments involving cell sorting and RNA sequencing. B.N. performed the bioinformatics data analysis and contributed to the editing of the manuscript. Y-Z.L. contributed to immunostaining and flow cytometry experiments. E.S. provided expert guidance for the left coronary artery ligation surgeries and provided instrumental support throughout the project. S.N.L. performed cryosectioning and paraffin sectioning. J.T. helped with initial development of the study. D.A-Z. performed protocol development and optimisation, data generation, and study design of the minibulk RNA sequencing. P.F.H. performed study design, data processing and QC of the minibulk RNA sequencing data. G.dM.-N. provided guidance on heart biology and helped with conceptualisation of the TUNEL experiment. A.V. provided expert guidance on Tregs and helped conceptualise the RNA sequencing experiments. Y.K.A. and M.M.M. wrote the initial manuscript draft and made the figures. Y.K.A. B.N., and M.M.M. edited the manuscript.

Competing interests

The authors declare no competing interests.

Additional information

Supplementary information The online version contains supplementary material available at https://doi.org/10.1038/s41467-024-50806-y.

Correspondence and requests for materials should be addressed to Mikaël M. Martino.

Peer review information *Nature Communications* thanks the anonymous, reviewers for their contribution to the peer review of this work. A peer review file is available.